Time-resolved Fourier-transform infrared emission spectroscopy of Ag in the (1300–3600)-cm^{-1} region: Transitions involving f and g states and oscillator strengths

S. Civiš,* I. Matulková, J. Cihelka, and P. Kubelik
J. Heyrovský Institute of Physical Chemistry, Academy of Sciences of the Czech Republic, Dolejškova 3, CZ-18223 Prague 8, Czech Republic

K. Kawaguchi
Faculty of Science, Okayama University, Tsushima-naka, Okayama 700-8530, Japan

V. E. Chernov
Voronezh State University, 394693 Voronezh, Russia
(Received 30 May 2010; published 3 August 2010)

We report on a study of the emission spectra of Ag vapor in a vacuum (10^{-2} Torr) formed in ablation of an Ag metal target by a high-repetition rate (1.0 kHz) pulsed nanosecond ArF laser ($\lambda = 193$ nm, output energy of 15 mJ). The time-resolved infrared emission spectrum of Ag was recorded in the 1300- to 3600-cm^{-1} spectral region using the Fourier transform infrared spectroscopy technique with a resolution of 0.02 cm^{-1}. The time profiles of the measured lines have maxima at 5–6 μs after a laser shot and display nonexponential decay with a decay time of 3–7 μs. The lines reported here are given with an uncertainty of 0.0005–0.016 cm^{-1}. The line classification is performed using relative line strengths expressed in terms of transition dipole matrix elements calculated with the help of the Fues model potential; these calculations show agreement with the large experimental and calculated data sets available in the literature. In addition to these data we also calculate transition probabilities and line and oscillator strengths for a number of transitions in the 1300- to 5000-cm^{-1} range between $(4d^{10})nl_j$ states of Ag.

DOI: 10.1103/PhysRevA.82.022502 PACS number(s): 32.30.Bv, 52.38.Mf, 07.57.Ty, 31.15.B−

I. INTRODUCTION

Silver has been observed in stellar spectra for several decades. The solar abundance of AgI has been evaluated based on measurements of the 3280.7 Å and 3382.9 Å lines [1]. The neutral silver 3382.9 Å line was detected in the spectra of stars of Se [2] and Ap type (e.g., the 4210.94 Å and 4668.48 Å lines in the Cr-Eu-Sr subgroup star [3] and the 5209.1 Å and 5465.5 Å lines in a Przybylski's star [4]). The AgI abundances obtained from 3382.9 Å and 3280.7 Å line measurements in metal-poor halo stars [5,6] were employed to study the processes of the chemical evolution of the Galaxy. For the correct interpretation of high-resolution astrophysical spectra, improved accuracy is required for atomic-level energies and transition probabilities (or oscillator strengths) data [7,8], including the infrared (IR) spectral region [9]. Infrared astronomy is very promising in studies of dust-obscured objects and interstellar clouds, cool objects such as brown dwarfs, and objects at cosmological distances from Earth [10].

Although the spectra of Ag have been studied for some decades [11–27], only a few lines in the IR region have been reported since a century ago: the two lines 2502.4 and 2506.3 cm^{-1} [11] and seven lines in the 5438–13004 cm^{-1} range [12]. One of the present work's aims is to supply information on Ag spectra in the 1300- to 3600-cm^{-1} range. This article continues our study of the IR spectra of metals started in Ref. [28].

The terms of the neutral Ag atom can be classified according to the $4d$ core state. The simplest level structure originates from the closed $4d^{10}$ core yielding $(4d^{10})nl_j$ states with a total angular momentum $J = j = l \pm \frac{1}{2}$ [13,16,19,25,26]. Other terms arise due to excitation of a $4d$ electron into a $n'l'$ state yielding $4d^9 5sn's$ [13,15,16,22,24,25], $4d^9 5sn'p$ [16–23,25,27], $4d^9 5sn'd$ [16,18,22], and $4d^9 5sn'f$ [20,23,27] states. These states are treated in terms of LS coupling with parentage schemes $4d^9(^3D_{J_{\rm II}})5s(^{1,3}D_{1,2,3})n'l'[^{2S+1}L_J]$ (Refs. [13,15,16,18–20,22,24,25]) or $5s5p(^{1,3}P_{J_{\rm I}})4d^{10}[^{2S+1}L_J]$ (Refs. [17,21]) as well as jj coupling $[(5s5p)_{J_{\rm I}}(4d^{10})_{J_{\rm II}}]_J$ (Ref. [17]) or the J_cK coupling scheme $4d^9 5s(^{1,3}D_{1,2,3})n'l'[K]_J$ (with $l' = 1,3$ [23,27]). The level diagrams of Ag can be found in Refs. [20,24,25].

One of the first comprehensive lists of Ag lines and term values was published by Shenstone [16]. Together with the results of his own measurements in the 40000- to 1250 Å (2500- to 80,000 cm^{-1}) range using an arc and hollow cathode lamp, Shenstone reported some lines observed previously by other researchers [11–14]. In the same year Rasmussen [15] reported values of some new levels, including the $4d^9 5s^2[^2D_{\frac{3}{2},\frac{5}{2}}]$ metastable doublet. More than 30 years later these data were extended by Johannsen and Linke's measurements of the Ag arc spectrum in the 1100 to 9800 Å range yielding values for some core-excited $4d^9 5sn'l'$ levels with $l' = 0,1,2$. The core-excited $4d^9 n'l'$ states were studied both by numerical *ab initio* calculations [17] and by VUV photoabsorption [19–23,27]; for $n' \geqslant 5$ or $l' \geqslant 2$ these levels correspond to autoionizing states lying above the first ionization threshold of Ag.

The most comprehensive reports of the closed-core $(4d^{10})nl_j$ states of Ag were made by Brown and Ginter [19] for np states up to $n = 71$ and by MacAdam *et al.* [26]

*Corresponding author: e-mail: civis@jh-inst.cas.cz

 ©2010 The American Physical Society

for s, p, and d states for $n = 28 - 39$. The most accurate values of $(4d^{10})nl_j$ level energies for $n \leqslant 10$ (as well as $4d^9 5s^2 {}^2D_{\frac{3}{2},\frac{5}{2}}$ and $4d^9 5s({}^3D_3)[{}^4P_{\frac{3}{2}\frac{5}{2}}]$ level energies) were presented by Pickering and Zilio [25] and therefore we use their level energies as "reference" values in the identification of the IR lines measured in this work (see subsection IV B below).

However, due to the great number of Rydberg levels populated in the conditions of a laser ablated plasma, the above information on Ag levels is not always sufficient for correct classification of the observed IR emission lines. While the $(4d^{10})nl$ level energies for $l \leqslant 2$ can be obtained by interpolation of the above cited data sources, such interpolation is impossible for f and g levels (i.e., $l = 3,4$) since their energies are known for only one or two n values ($n = 4,5$ for f states and $n = 5$ for the g state without fine structure) obtained 70 years ago [16]. To identify the transitions involving these and other low-Rydberg Ag levels, we use the information on the relative intensity of the transitions between Ag $(4d^{10})nl$ levels. Such information is obtained here by the calculation of dipole transition matrix elements (or transition dipole moments) using the Fues model potential (FMP) approach (see Sec. III).

The transition dipole moments for the Ag atom have been studied for some decades both theoretically and experimentally, and in the literature they are most frequently reported as oscillator strengths. Direct experimentally measured data on oscillator strengths in Ag, to our knowledge, are available mostly for the resonance doublet, i.e., for the $5s_{\frac{1}{2}} - 5p_{\frac{1}{2},\frac{3}{2}}$ transitions. The oscillator strengths for these transitions were obtained by Hinnov and Kohn [29] from the measured density dependence of the intensity of the atomic lines emitted by an acetylene-air flame; this dependence is determined by the cross section of the collisional interaction between the emitting atoms with foreign molecules (optical cross section). Some years later, the oscillator strengths for the Ag resonance doublet were measured: by Penkin and Slavenas [30] using the anomalous dispersion curves (Rozhdestvenskii hook method); by Lawrence, Link, and King [31] using the atomic-beam technique; by Moise [32] using curves of growth in the furnace absorption tube along with vapor-pressure data; by Levin and Budick [33] using level-crossing spectroscopy (Hanle effect); by Klose [34] using delayed coincidence with excitation of the $5p_{\frac{3}{2}}$ level by a tunable dye laser; by Selter and Kunze [35] with direct observation of the exponential decay of the $5p_{\frac{3}{2}}$ level excited by a pulsed dye laser; by Hannaford and Lowe [36] using laser-induced fluorescence on an uncollimated atomic beam; and by Soltanolkotabi and Gupta [37] using level-crossing spectroscopy (Hanle effect).

The most accurate measurement of the oscillator strengths for the Ag resonance doublet was performed by Carlsson, Jonsson, and Sturesson [38] using time-resolved laser spectroscopy with delayed coincidence technique. A review of experimental methods for the determination of oscillator strengths of resonance atomic lines was presented by Doidge [39]. A critical compilation of oscillator strengths for 2249 spectral lines arising from the ground states of atoms and ions for astronomy needs is given in Ref. [40].

The experimental data on f values for the transition between excited states are scarce. The oscillator strengths for the second doublet $5s_{\frac{1}{2}} - 6p_{\frac{1}{2},\frac{3}{2}}$ were measured by Slavenas [41] using the Rozhdestvenskii hook method. The radiative lifetimes of the $(4d^{10})nd_{\frac{3}{2},\frac{5}{2}}$ and $(4d^{10})ns_{\frac{1}{2}}$ levels (and some core-excited states) of Ag were measured by Plekhotkina [42] using delayed coincidence with electron-beam excitation for n up to 8. Zhankui *et al.* [43] measured the lifetimes of the $(4d^{10})nd_{\frac{3}{2}}$ and $(4d^{10})ns_{\frac{1}{2}}$ states with n up to 10 by direct recording of time-resolved fluorescence decay curves with selective stepwise excitation using two pulsed dye lasers. Bengtsson *et al.* measured the lifetimes of the $(4d^{10})6p_{\frac{1}{2},\frac{3}{2}}$ [44] and $(4d^{10})7p_{\frac{1}{2},\frac{3}{2}}$ [45] states using both level-crossing and time-resolved spectroscopy methods.

One of the first theoretical calculations of oscillator strengths in the Ag isoelectronic series was performed by Cheng and Kim [46] using the multiconfiguration Hartree-Fock method (RHF) and by Migdałek and Baylis [47–50] using single-configuration RHF combined with relativistic model potential (RMP) methods. The latter methods were based on local approximations for the valence electron's exchange interaction [50] (these approximations will be denoted by roman numerals in the further comparison with present work calculations). Moreover, these authors also considered the core-polarization (CP) effects by the mean of one-electron dipole potential of the core due to its static polarizability. The influence of this potential on the oscillator strengths both *via* the valence electron wave functions and via the dipole transition operator was studied separately [48]. The above dipole potential was regularized at small distances using an effective core radius r_0 which was set equal to the mean radius of the outermost core orbital or the value was adjusted to match experimental energy levels; these cases are denoted as (A) and (B) correspondingly in the further comparison with the results of Migdałek and Baylis.

The effect of the induced dipole moment of the core (due to its dynamic polarizability) on the oscillator strengths was studied by Chichkov and Shevelko [51] using a Coulomb-like approximation for radial matrix elements for the dipole transition of the valence electron. A variant of the Coulomb-like approximation, the quantum-defect orbital (QDO) method, was used by Martín, Almaraz, and Lavin [52,53] for the calculation of oscillator strengths for Ag isoelectronic series with an account for relativistic (RQDO) and CP effects. As will be shown below, the Coulomb-like approximation [including the Fues model potential (FMP) exploited in this work] gives good results for the Ag oscillator strengths. For the majority of the transition studied, the Coulomb-like approximation gives results close to those of *ab initio* calculations.

One of recent *ab initio* studies of oscillator strengths for the Ag isoelectronic series was performed by Migdałek and Garmulewicz [54] using single-configuration Dirac-Fock (DF) with an account for exchange by local model potentials (denoted as DX with a roman numeral enumerating their types). Safronova, Savukov, and Johnson [55] performed calculations of oscillator strengths, transition probabilities, level energies, and lifetimes in Ag isoelectronic series using third-order relativistic many-body perturbation theory

TABLE I. Oscillator strengths ($f \times 100$) and wavelengths for $5s \rightarrow 5p$ transitions in Ag. CP means an account for core polarization, (P) and (T) means CP account in the potential and in transition matrix element; I–IV denote different variants for local exchange potential; (A) and (B) denote different variants of effective core radius choice (see text for more details).

	$5s_{\frac{1}{2}} \rightarrow 5p_{\frac{1}{2}}$		$5s_{\frac{1}{2}} \rightarrow 5p_{\frac{3}{2}}$	
Method	λ (Å)	$f \times 100$	λ (Å)	$f \times 100$
Optical cross section [29]	3383.	22.	3281.	39.
Rozhdestvenskii hook [30]		24.7(4)		50.6(4)
Atomic beam [31]	3382.89	21.5(22)	3280.68	45.0(45)
Absorption tube [32]	3383.	19.6(15)	3280.	45.9(34)
Hanle effect [33][a]				43.7(41)
Delayed coincidence [34][a]				49.7(50)
Laser-ind. fluoresc. [35]			3280.7	44.(2)
Laser-ind. fluoresc. [36][a]		25.3(11)		51.3(16)
Hanle effect [37][a]		22.7(7)		50.9(14)
Del. coincidence [38][a]		23.2(1)		47.6(2)
From compil. tables [40]	3283.836	21.0	3281.627	45.2
RHF [46]	4126.	32.9	4025.	66.6
RHF [47]		40.3		82.2
RHF + CP [47]		19.8		41.3
RMPI [48]	3383.86	32.9	3281.5	67.2
RMPI + CP(A) [48]	3383.86	21.5	3281.5	44.6
RHF + CP(P) [49]		34.0		69.5
RHF + CP(PT) [49]		21.4		44.5
RMPII [50]		34.4		70.2
RMPII + CP(A) [50]		20.8		43.4
RMPI + CP(B) [50]		19.6		41.0
RMPII + CP(A) [50]		22.1		46.0
RMPII + CP(B) [50]		21.3		44.4
QDO [53]		22.713		45.425
RQDO [53]		22.402		45.714
RQDO + CP [53]		19.400		39.674
DXI + CP [54]		21.4		44.5
DXIII + CP [54]		23.5		48.6
DXIV + CP [54]		23.7		48.9
DF + CP [54]		22.2		46.2
RMBPT [55]	3562.14	24.97	3454.71	51.34
MCHF + BP [56]	4157.67	37.204	4073.05	36.3846
FMP (this work)	3383.85	27.9	3281.626	57.2

[a]The f values are extracted from the reported lifetimes according to the Eqs. (2) and (3) using FMP-calculated ratios.

(RMBPT). Özdemir, Karaçoban, and Ürer [56] calculated oscillator strengths and transition probabilities in neutral Ag using the multiconfiguration Hartree-Fock method with Breit-Pauli relativistic correction (MCHF + BP).

In the present work oscillator and line strengths are calculated using the FMP approach briefly sketched in Sec. III. The comparison tables presented in subsection IV A show reasonable agreement of our calculations with the above experimental and numerical results. The line strengths calculated for the transitions in the 1300- to 5000-cm^{-1} range are used in subsection IV B for classification of the observed lines resulting in revised values for some terms of neutral Ag. The experimental setup has already been published in detail in our previous articles [28,57] and therefore the following section gives a brief description only. All the uncertainties are given in round brackets after the corresponding values and should be treated as their rightmost significant digits, e.g., 112.8(72) means 112.8 ± 7.2.

II. EXPERIMENTAL

Time-resolved Fourier-transform infrared (FTIR) spectroscopy was applied for observations of the emission arising after the irradiation of metals with a pulsed nanosecond ArF ($\lambda = 193$ nm) laser at fluences between 2 and 20 J/cm^2. A high-repetition-rate ArF laser ExciStar S-Industrial V2.0 1000 (193 nm, laser pulse width 12 ns, frequency 1 kHz) with 15-mJ output power was focused on a rotating and linearly traversing silver target inside a vacuum chamber (average pressure 10^{-2} Torr).

The time-resolution FTIR spectra were measured using the Bruker IFS 120 HR spectrometer (modified for the

TABLE II. Oscillator strengths ($f \times 100$) for $5p \rightarrow ns$ transitions in Ag. For description of the methods see Table I and text.

Method	$5p \rightarrow 6s$		$5p \rightarrow 7s$		$5p \rightarrow 8s$		$5p \rightarrow 9s$		$5p \rightarrow 10s$	
$J_l \rightarrow J_u$	$\frac{1}{2} \rightarrow \frac{1}{2}$	$\frac{3}{2} \rightarrow \frac{1}{2}$	$\frac{1}{2} \rightarrow \frac{1}{2}$	$\frac{3}{2} \rightarrow \frac{1}{2}$	$\frac{1}{2} \rightarrow \frac{1}{2}$	$\frac{3}{2} \rightarrow \frac{1}{2}$	$\frac{1}{2} \rightarrow \frac{1}{2}$	$\frac{3}{2} \rightarrow \frac{1}{2}$	$\frac{1}{2} \rightarrow \frac{1}{2}$	$\frac{3}{2} \rightarrow \frac{1}{2}$
Delayed coincidence [42][a]			1.69(13)	1.58(18)	0.338(32)	0.311(29)				
Laser-ind. fluoresc. [43][a]	14.5(19)	14.9(20)	1.32(12)	1.23(12)	0.480(50)	0.441(45)	0.224(19)	0.205(17)	0.120(8)	0.109(7)
RMPI [48]	14.5	15.4	1.50	1.46						
RMPI + CP(A) [48]	15.7	16.6	1.58	1.53						
RHF [50]	21.6	22.4	1.68	1.59	0.535	0.501	0.248	0.231		
RMPI [50]	14.5	15.4	1.50	1.46	0.504	0.488	0.239	0.230		
RMPII [50]	15.2	16.2	1.60	1.57	0.532	0.513	0.251	0.240		
RHF + CP [50]	15.8	16.7	1.68	1.61	0.574	0.542	0.273	0.257		
RMPI + CP(A) [50]	16.0	16.8	1.69	1.62	0.573	0.540	0.273	0.255		
RMPI + CP(B) [50]	16.1	16.9	1.72	1.65	0.589	0.552	0.282	0.262		
RMPII + CP(A) [50]	15.9	16.8	1.65	1.58	0.557	0.528	0.264	0.249		
RMPII + CP(B) [50]	15.7	16.6	1.66	1.58	0.557	0.524	0.264	0.248		
DXI + CP [54]	16.1	17.0								
DXIII + CP [54]	15.4	16.5								
DXIV + CP [54]	17.0	17.7								
DF + CP [54]	16.1	17.0								
MCHF + BP [56]	0.763	1.05	0.443	0.904						
FMP (this work)	16.6	17.1	1.49	1.38	0.480	0.441	0.222	0.203	0.123	0.112

[a]The f values are extracted from the reported lifetimes according to the Eqs. (2) and (3) using FMP-calculated ratios.

TABLE III. Oscillator strengths ($f \times 10^4$) for $5s \to np$ transitions in Ag. For description of the methods see Table I and text.

Method	$5s \to 6p$		$5s \to 7p$		$5s \to 8p$		$5s \to 9p$		$5s \to 10p$	
$J_l \to J_u$	$\frac{1}{2} \to \frac{1}{2}$	$\frac{1}{2} \to \frac{3}{2}$	$\frac{1}{2} \to \frac{1}{2}$	$\frac{1}{2} \to \frac{3}{2}$	$\frac{1}{2} \to \frac{1}{2}$	$\frac{1}{2} \to \frac{3}{2}$	$\frac{1}{2} \to \frac{1}{2}$	$\frac{1}{2} \to \frac{3}{2}$	$\frac{1}{2} \to \frac{1}{2}$	$\frac{1}{2} \to \frac{3}{2}$
Hook [41]	11.(2)	45.(8)								
Laser-ind. fluoresc. [44,45][a]	45.1(29)	112.8(72)	13.5(12)	30.9(24)						
MCHF [44][a]	110.	258.8								
From compil. tables [40]	9.64	39.5								
RHF [50]	110.	289.	23.4	67.2	8.82	26.6	4.34	13.4		
RMPI [50]	57.3	167.	10.6	35.4	3.75	13.4	1.77	6.62		
RMPII [50]	66.1	188.	13.6	43.3	5.10	17.1	2.50	8.65		
RHF + CP [50]	5.91	32.9	0.00965	2.24	0.0808	0.279	0.118	0.0419		
RMPI + CP(A) [50]	4.34	27.5	0.0344	1.24	0.247	0.0578	0.258	0.00033		
RMPI + CP(B) [50]	1.35	16.3	0.652	0.847	0.898	0.0129	0.726	0.28		
RMPII + CP(A) [50]	8.22	40.3	0.112	3.48	0.0153	0.613	0.0498	0.156		
RMPII + CP(B) [50]	3.93	27.0	0.0599	1.18	0.291	0.0485	0.293	0.00118		
MP + BP [51]	3.6	23.	0.48	0.051	1.1	0.31	1.0	0.53		
QDO [53]	128.9	257.7	37.0	74.0	16.0	32.1	8.5	16.9	5.1	10.2
RQDO [53]	117.0	269.9	33.2	77.9	14.3	33.9	7.6	17.9	4.5	10.9
RQDO + CP [53]	86.5	203.5	23.2	56.0	9.8	23.8	5.1	12.4	3.0	7.5
MCHF + BP [56]	0.7605	75.95								
FMP (this work)	111.	265.	28.4	70.1	11.7	29.2	6.0	15.0	3.51	9.07

[a]The f values are extracted from the reported lifetimes according to Eqs. (2) and (3) using FMP-calculated ratios.

TABLE IV. Oscillator strengths ($f \times 100$) for $5p \to nd$ transitions in Ag. For description of the methods see Table I and text.

Method	$5p \to 5d$			$5p \to 6d$			$5p \to 7d$			$5s \to 8d$			$5p \to 9d$		
$J_l \to J_u$	$\frac{1}{2} \to \frac{3}{2}$	$\frac{3}{2} \to \frac{3}{2}$	$\frac{3}{2} \to \frac{5}{2}$	$\frac{1}{2} \to \frac{3}{2}$	$\frac{3}{2} \to \frac{3}{2}$	$\frac{3}{2} \to \frac{5}{2}$	$\frac{1}{2} \to \frac{3}{2}$	$\frac{3}{2} \to \frac{3}{2}$	$\frac{3}{2} \to \frac{5}{2}$	$\frac{1}{2} \to \frac{3}{2}$	$\frac{3}{2} \to \frac{3}{2}$	$\frac{3}{2} \to \frac{5}{2}$	$\frac{1}{2} \to \frac{3}{2}$	$\frac{3}{2} \to \frac{3}{2}$	$\frac{3}{2} \to \frac{5}{2}$
Delayed coincidence [42][a]	53.1(3.3)	5.52(3)		11.3(12)	1.12(12)		4.18(38)	0.407(37)	3.97(28)						
Laser-ind. fluoresc. [43] [a]	62.3(170)	6.48(177)		13.1(20)	1.30(20)		4.22(41)	0.411(40)		2.17(16)	0.210(16)		1.20(9)	0.115(8)	
RHF [46]	71.1		66.9												
RHF [47]	88.2	9.1	22.0												
RHF + CP [47]	56.2	6.0	53.2												
RMPI [48]	60.2	6.35	56.9	13.3	1.33	11.9									
RMPI + CP [48]	55.8	5.92	53.0	11.4	1.16	10.4									
RHF [49]	88.2	9.15	82.0												
RHF + CP(P) [49]	61.8	6.53	58.5												
RHF + CP(PT) [49]	56.5	5.99	53.6												
RHF [50]	88.2	9.15	82.0	15.5	1.52	13.7	5.72	0.550	4.97	2.81	0.267	2.42	1.61	0.152	1.38
RMPI [50]	60.2	6.35	56.9	13.3	1.33	12.0	5.21	0.509	4.60	2.63	0.254	2.30	1.52	0.146	1.33
RMPII [50]	61.3	6.49	5.79	13.1	0.131	11.8	5.06	0.498	4.48	2.54	0.247	2.23	1.47	0.142	1.29
RHF + CP [50]	56.4	5.98	53.6	11.5	1.16	10.4	4.4	0.435	3.94	2.21	0.215	1.95	1.28	0.123	1.12
RMPI + CP(A) [50]	55.9	5.93	53.1	11.4	0.114	10.3	4.33	0.425	3.84	2.15	0.209	1.89	1.24	0.120	1.08
RMPI + CP(B) [50]	55.2	5.86	52.4	11.2	1.12	10.1	4.24	0.417	3.77	2.10	0.205	1.85	1.21	0.117	1.06
RMPII + CP(A) [50]	56.3	5.97	53.5	11.4	1.12	10.3	4.35	0.428	3.87	2.16	0.211	1.91	1.25	0.121	1.09
RMPII + CP(B) [50]	55.0	5.86	52.4	11.2	1.12	10.1	4.25	0.418	3.77	2.11	0.206	1.86	1.21	0.117	1.07
QDO [52]	61.19	6.12	55.08	13.13	1.31	11.81	5.16	0.52	4.65	2.62	0.26	2.35	1.52	0.15	1.37
RQDO [52]	59.69	6.20	55.75	13.18	1.31	11.78	5.23	0.51	4.61	2.66	0.26	2.33	1.56	0.15	1.36
RQDO + CP [52]	54.60	5.69	51.16	11.47	1.14	10.28	4.44	0.43	3.92	2.23	0.22	1.95	1.29	0.12	1.13
DXI + CP [54]	56.4	6.1	54.2												
DXIII + CP [54]	50.4	5.5	49.1												
DXIV + CP [54]	66.3	6.9	62.0												
DF + CP [54]	58.3	5.6	55.5												
RMBPT [55]	57.73	6.13	54.91												
MCHF + BP [56]	1.97077	0.385625	2.3042	1.0736	0.210415	1.2734									
FMP (this work)	59.7	6.20	55.8	13.2	1.31	11.8	5.23	0.510	4.61	2.66	0.257	2.33	1.56	0.150	1.36

[a]The f values are extracted from the reported lifetimes according to the Eqs. (2) and (3) using FMP-calculated ratios.

TABLE V. Comparison of oscillator strengths ($f \times 100$) in Ag calculated using quantum-defect orbitals (Ref. [53] for $6s \rightarrow np$ transitions and Ref. [52] for $5p \rightarrow 10d$ transitions; see also the Tables I and IV) with the present FMP calculation and the laser-induced measurement of the radiative lifetimes of $6s_{\frac{1}{2}}$ [44] and $7s_{\frac{1}{2}}$ [45] levels (the f values are extracted by Eqs. (2) and (3) using FMP-calculated ratios).

Transition	QDO	RQDO	RQDO + CP	Expt.	FMP (this work)
$6s_{\frac{1}{2}} \rightarrow 6p_{\frac{1}{2}}$	39.480	39.234	38.572	16.0(10)	39.3
$6s_{\frac{1}{2}} \rightarrow 6p_{\frac{3}{2}}$	78.960	79.156	77.865	33.8(22)	79.2
$6s_{\frac{1}{2}} \rightarrow 7p_{\frac{1}{2}}$	1.737	1.545	1.448	73.2(64)	1.54
$6s_{\frac{1}{2}} \rightarrow 7p_{\frac{3}{2}}$	3.474	3.671	3.465	1.62(13)	3.67
$6s_{\frac{1}{2}} \rightarrow 8p_{\frac{1}{2}}$	0.450	0.389	0.355		0.390
$6s_{\frac{1}{2}} \rightarrow 8p_{\frac{3}{2}}$	0.900	0.963	0.886		0.964
$6s_{\frac{1}{2}} \rightarrow 9p_{\frac{1}{2}}$	0.188	0.162	0.144		0.161
$6s_{\frac{1}{2}} \rightarrow 9p_{\frac{3}{2}}$	0.376	0.403	0.365		0.403
$6s_{\frac{1}{2}} \rightarrow 10p_{\frac{1}{2}}$	0.100	0.084	0.074		0.084
$6s_{\frac{1}{2}} \rightarrow 10p_{\frac{3}{2}}$	0.201	0.218	0.196		0.218
$5p_{\frac{1}{2}} \rightarrow 10d_{\frac{1}{2}}$	0.97	0.99	0.82		0.994
$5p_{\frac{3}{2}} \rightarrow 10d_{\frac{3}{2}}$	0.10	0.10	0.08		0.0954
$5p_{\frac{3}{2}} \rightarrow 10d_{\frac{5}{2}}$	0.88	0.87	0.71		0.866

time-resolution scan of emission data) in a spectral range of 1800–6000 cm^{-1} using a CaF_2 beam splitter and InSb detector. In the 1200- 1800-cm^{-1} spectral range a mercury-cadmium-telluride (MCT) detector was used. The infrared emission (axial distance from the target 10 mm) was focused into the spectrometer using a CaF_2 lens.

For data sampling, we used so-called 1/3 sampling [28], where the scanner velocity was set to produce a 3-kHz He-Ne laser interference signal, and the ArF laser oscillation was triggered at one-third of the He-Ne frequency. Measurements were carried out with a resolution of 0.02 cm^{-1} and three scans were needed to complete the interferogram. Three to thirty scans were usually coadded to obtain a reasonable signal-to-noise ratio (SNR). The infrared emission was observed in the 1800- to 3600-cm^{-1} (with MID IR interference filter) spectral region with a time profile showing maximum emission intensity in 5–6 μs after a laser shot. The acquired spectra and accumulated line profiles were postzero filled by a factor of 4 and analyzed using using a commercial software routine (Bruker OPUS version 3.1) [58]. Subsequently, the spectra were corrected by subtracting the blackbody background spectrum.

III. TRANSITION DIPOLE MOMENTS: THE FUES MODEL POTENTIAL CALCULATION

Under thermal equilibrium conditions, the intensity of a spectral line due to radiative transition from the upper state $|k\rangle$ to the lower state $|i\rangle$ is proportional to the transition probability $A_{k\rightarrow i}$ [59]:

$$I_{k\rightarrow i} \sim g_k A_{k\rightarrow i} \omega_{ik} e^{-E_k/T}, \tag{1}$$

where E_k and g_k are the upper level's excitation energy and degeneracy factor, respectively, $\omega_{ik} = E_k - E_i$ is the transition frequency and T is the temperature. In the majority of experimental works the transition probability, $A_{k\rightarrow i}$, is determined by measurements of the upper level's lifetime, τ_k:

$$\tau_k = \sum_l A^{-1}_{k\rightarrow i}. \tag{2}$$

If the probabilities of transitions other than the $|k\rangle \rightarrow |i\rangle$ transition are not significant then $\tau_k = A^{-1}_{k\rightarrow i}$. This is the case for the Ag resonance doublet, i.e., for $|k\rangle = |5p_{\frac{1}{2},\frac{3}{2}}\rangle$. The probabilities $A_{k\rightarrow i}$ for the electric dipole $|k\rangle \rightarrow |i\rangle$ transition can be expressed in terms of oscillator strengths [39]:

$$f_{i\rightarrow k} = \frac{m_e c^2}{2\alpha\hbar\omega^2_{ik}} \frac{g_k}{g_i} A_{k\rightarrow i} = \frac{m_e c \lambda^2_{ik}}{8\pi^2 e^2} \frac{g_k}{g_i} A_{k\rightarrow i}$$
$$\simeq 1.50 \times 10^{-16} \lambda^2_{ik} \frac{g_k}{g_i} A_{k\rightarrow i}. \tag{3}$$

Here m_e and e are the electron mass and charge, c is the light velocity, $\alpha = \frac{e^2}{\hbar c} \simeq 1/137.036$ is the fine-structure constant, $\hbar$ is the Planck constant, and λ_{ik} is the transition wavelength. If the hyperfine structure is not taken into account, the degeneracy factor $g_s = 2J_s + 1$ is determined by the total angular momentum, J_s $(s = i,k)$. The last numerical expression (3) assumes $A_{k\rightarrow i}$ to be measured in s^{-1} and λ_{ik} in Ångströms.

In our analysis of the relative line intensities it is convenient to use the line strengths

$$S_{i\rightarrow k} = \frac{3\hbar e^2 g_i}{2m_e \omega_{ik}} f_{i\rightarrow k} \tag{4}$$

since, according to Eq. (1), the line intensity is proportional to the S value.

The above f, A, and S values can be expressed in terms of a dipole transition matrix element (so-called transition dipole moment). The wave function of an atomic state with one

TABLE VI. Comparison of oscillator strengths ($f \times 100$) for transitions from np states in Ag ($n = 5 - 10$) with the data extracted from the experimental lifetimes ns and nd levels [42,43] with the help of Eqs. (2) and (3) using FMP-calculated ratios).

Transition	[42]	[43]	FMP (this work)	Transition	[42]	[43]	FMP (this work)
$6p_{\frac{1}{2}} \to 7s_{\frac{1}{2}}$	36.3(28)	28.6(27)	32.2	$8p_{\frac{1}{2}} \to 9s_{\frac{1}{2}}$		61.2(52)	60.7
$6p_{\frac{3}{2}} \to 7s_{\frac{1}{2}}$	37.2(29)	29.1(28)	32.7	$8p_{\frac{3}{2}} \to 9s_{\frac{1}{2}}$		62.9(53)	61.6
$6p_{\frac{1}{2}} \to 8s_{\frac{1}{2}}$	1.64(15)	2.33(24)	2.33	$8p_{\frac{1}{2}} \to 10s_{\frac{1}{2}}$		3.86(26)	3.96
$6p_{\frac{3}{2}} \to 8s_{\frac{1}{2}}$	1.50(14)	2.12(22)	2.12	$8p_{\frac{3}{2}} \to 10s_{\frac{1}{2}}$		3.48(23)	3.57
$6p_{\frac{1}{2}} \to 9s_{\frac{1}{2}}$		0.731(62)	0.726	$8p_{\frac{1}{2}} \to 7d_{\frac{3}{2}}$	15.1(14)	15.3(15)	18.9
$6p_{\frac{3}{2}} \to 9s_{\frac{1}{2}}$		0.654(55)	0.649	$8p_{\frac{3}{2}} \to 7d_{\frac{3}{2}}$	0.748(68)	0.755(74)	0.936
$6p_{\frac{1}{2}} \to 10s_{\frac{1}{2}}$		0.328(22)	0.336	$8p_{\frac{3}{2}} \to 7d_{\frac{5}{2}}$	8.32(59)		9.68
$6p_{\frac{3}{2}} \to 10s_{\frac{1}{2}}$		0.291(19)	0.299	$8p_{\frac{1}{2}} \to 8d_{\frac{3}{2}}$		40.5(31)	49.6
$6p_{\frac{1}{2}} \to 5d_{\frac{3}{2}}$	8.10(50)	9.50(259)	9.10	$8p_{\frac{3}{2}} \to 8d_{\frac{3}{2}}$		4.54(35)	5.56
$6p_{\frac{3}{2}} \to 5d_{\frac{3}{2}}$	0.438(27)	0.514(140)	0.492	$8p_{\frac{1}{2}} \to 9d_{\frac{3}{2}}$		10.6(8)	13.8
$6p_{\frac{1}{2}} \to 6d_{\frac{3}{2}}$	43.5(48)	50.5(78)	50.8	$8p_{\frac{3}{2}} \to 9d_{\frac{3}{2}}$		1.13(8)	1.47
$6p_{\frac{3}{2}} \to 6d_{\frac{3}{2}}$	4.70(51)	5.46(84)	5.49	$9p_{\frac{1}{2}} \to 10s_{\frac{1}{2}}$		72.7(48)	74.6
$6p_{\frac{1}{2}} \to 7d_{\frac{3}{2}}$	10.4(9)	10.5(10)	13.0	$9p_{\frac{3}{2}} \to 10s_{\frac{1}{2}}$		73.7(49)	75.6
$6p_{\frac{3}{2}} \to 7d_{\frac{3}{2}}$	1.07(10)	1.08(11)	1.34	$9p_{\frac{1}{2}} \to 8d_{\frac{3}{2}}$		19.3(15)	23.6
$6p_{\frac{3}{2}} \to 7d_{\frac{5}{2}}$	10.4(7)		12.0	$9p_{\frac{3}{2}} \to 8d_{\frac{3}{2}}$		0.983(76)	1.20
$6p_{\frac{1}{2}} \to 8d_{\frac{3}{2}}$		4.51(35)	5.53	$9p_{\frac{1}{2}} \to 9d_{\frac{3}{2}}$		39.2(30)	50.9
$6p_{\frac{3}{2}} \to 8d_{\frac{3}{2}}$		0.456(35)	5.59	$9p_{\frac{3}{2}} \to 9d_{\frac{3}{2}}$		4.42(34)	5.74
$6p_{\frac{1}{2}} \to 9d_{\frac{3}{2}}$		2.26(17)	2.93	$10p_{\frac{1}{2}} \to 9d_{\frac{3}{2}}$		21.8(17)	28.4
$6p_{\frac{3}{2}} \to 9d_{\frac{3}{2}}$		0.226(17)	0.294	$10p_{\frac{3}{2}} \to 9d_{\frac{3}{2}}$		0.976(74)	1.27
$7p_{\frac{1}{2}} \to 8s_{\frac{1}{2}}$	32.9(31)	46.7(48)	46.7	$4f_{\frac{5}{2}} \to 7d_{\frac{3}{2}}$	0.643(58)	0.649(64)	0.804
$7p_{\frac{3}{2}} \to 8s_{\frac{1}{2}}$	33.4(31)	47.4(48)	47.4	$4f_{\frac{5}{2}} \to 7d_{\frac{5}{2}}$	0.0475(33)		0.0553
$7p_{\frac{1}{2}} \to 9s_{\frac{1}{2}}$		3.17(27)	3.15	$4f_{\frac{7}{2}} \to 7d_{\frac{5}{2}}$	0.713(51)		0.830
$7p_{\frac{3}{2}} \to 9s_{\frac{1}{2}}$		2.87(24)	2.85	$4f_{\frac{5}{2}} \to 8d_{\frac{3}{2}}$		0.116(9)	0.142
$7p_{\frac{1}{2}} \to 10s_{\frac{1}{2}}$		0.942(62)	0.966	$4f_{\frac{5}{2}} \to 9d_{\frac{3}{2}}$		0.0385(29)	0.0501
$7p_{\frac{3}{2}} \to 10s_{\frac{1}{2}}$		0.835(55)	0.856	$5f_{\frac{5}{2}} \to 7d_{\frac{3}{2}}$	0.723(66)	0.730(72)	0.904
$7p_{\frac{1}{2}} \to 6d_{\frac{3}{2}}$	12.1(13)	14.1(22)	14.2	$5f_{\frac{5}{2}} \to 7d_{\frac{5}{2}}$	0.0934(66)		0.109
$7p_{\frac{3}{2}} \to 6d_{\frac{3}{2}}$	0.611(67)	0.709(109)	0.714	$5f_{\frac{7}{2}} \to 7d_{\frac{5}{2}}$	1.40(10)		1.63
$7p_{\frac{1}{2}} \to 7d_{\frac{3}{2}}$	39.3(3.6)	39.7(39)	49.2	$5f_{\frac{5}{2}} \to 8d_{\frac{3}{2}}$		1.66(13)	2.03
$7p_{\frac{3}{2}} \to 7d_{\frac{3}{2}}$	4.34(0.39)	4.39(43)	5.43	$5f_{\frac{5}{2}} \to 9d_{\frac{3}{2}}$		0.297(22)	0.386
$7p_{\frac{3}{2}} \to 7d_{\frac{5}{2}}$	41.6(29)		48.3	$6f_{\frac{5}{2}} \to 9d_{\frac{3}{2}}$		3.11(23)	4.04
$7p_{\frac{1}{2}} \to 8d_{\frac{3}{2}}$		10.9(9)	13.4				
$7p_{\frac{3}{2}} \to 8d_{\frac{3}{2}}$		1.15(9)	1.40				
$7p_{\frac{1}{2}} \to 9d_{\frac{3}{2}}$		4.52(34)	5.88				
$7p_{\frac{3}{2}} \to 9d_{\frac{3}{2}}$		0.466(35)	0.606				

electron over a closed core [such as the $(4d^{10})nl_j$ states in Ag] can be written as a Clebsch-Gordan sum

$$\langle r|nljm\rangle = R_{nlj}(r)\sum_{\mu\sigma}\left\langle l\mu\frac{1}{2}\sigma\middle|jm\right\rangle Y_{l\mu}(\hat{r})\chi_{\frac{1}{2}\sigma}. \qquad (5)$$

Then we have [59]:

$$\begin{aligned} A_{k\to i} &= \frac{8\alpha}{3c^2}\frac{\omega_{ik}^3}{2j_k+1}Q_{ki}l_{\max}|\mathcal{D}_{ki}|^2 \\ f_{i\to k} &= \frac{4m_e}{3\hbar}\frac{\omega_{ik}}{2j_i+1}Q_{ki}l_{\max}|\mathcal{D}_{ki}|^2 \qquad (6) \\ S_{i\to k} &= 2e^2Q_{ki}l_{\max}|\mathcal{D}_{ki}|^2, \quad l_{\max} = \max\{l_k,l_i\}, \end{aligned}$$

where the angular matrix element is expressed in terms of $6j$ symbols:

$$Q_{ik} = \frac{1}{2}(2j_i+1)(2j_k+1)\begin{Bmatrix} l_i & j_i & \frac{1}{2} \\ j_k & l_k & 1 \end{Bmatrix}^2.$$

We calculate the radial dipole matrix elements

$$\mathcal{D}_{ik} = \int_0^\infty drr^3R_{n_il_ij_i}(r)R_{n_kl_kj_k}(r) \qquad (7)$$

using the Fues model potential (FMP) [60,61]. This method has proved its efficiency for the calculation of atomic and molecular matrix elements of single [62] and higher [63] orders. The FMP approach is close to single-channel quantum defect theory which is also a simple and quantitatively

TABLE VII. Comparison of oscillator strengths involving nf and ng states calculated using different methods.

Transition	RHF [46]	RMBPT [55]	MCHF + BP [56]	FMP (this work)
$5d_{\frac{3}{2}} \rightarrow 4f_{\frac{5}{2}}$	1.073	1.0118		1.0094
$5d_{\frac{5}{2}} \rightarrow 4f_{\frac{5}{2}}$		0.0484		0.0481
$5d_{\frac{5}{2}} \rightarrow 4f_{\frac{7}{2}}$	1.015	0.9678		0.9622
$5d_{\frac{3}{2}} \rightarrow 5f_{\frac{5}{2}}$	0.150			0.1580
$5d_{\frac{5}{2}} \rightarrow 5f_{\frac{5}{2}}$				0.0075
$5d_{\frac{5}{2}} \rightarrow 5f_{\frac{7}{2}}$	0.141			0.1498
$4f_{\frac{5}{2}} \rightarrow 5g_{\frac{7}{2}}$	1.346	1.3800	1.1910	1.3438
$4f_{\frac{7}{2}} \rightarrow 5g_{\frac{7}{2}}$		0.0383	0.0441	0.0373
$4f_{\frac{7}{2}} \rightarrow 5g_{\frac{9}{2}}$	1.308	1.3405	1.2351	1.3065
$5f_{\frac{5}{2}} \rightarrow 5g_{\frac{7}{2}}$	0.003		0.2956	0.0174
$5f_{\frac{7}{2}} \rightarrow 5g_{\frac{7}{2}}$			0.0109	0.00048
$5f_{\frac{7}{2}} \rightarrow 5g_{\frac{9}{2}}$	0.002		0.3066	0.0169

adequate method for the calculation of first- [62] and second-order [64] matrix elements in atoms and molecules.

The radial wave function of the valence nl_j electron in FMP has a Coulomb-like form and can be expressed in terms of Whittaker functions, Gaussian hypergeometric functions or Laguerre polynomials [65]:

$$R_{nlj}(r) = \frac{2Z^{3/2}}{n^{*2}} \frac{N}{\Gamma(2l^*+2)} \frac{1}{x} M_{n^*,l^*+\frac{1}{2}}(x) = \frac{2Z^{3/2}}{n^{*2}} \frac{N x^{l^*} \mathrm{e}^{-x/2}}{\Gamma(2l^*+2)} {}_1F_1(-n_r, 2l^*+2; x) = \frac{2Z^{3/2}}{n^{*2}} \frac{1}{N} x^{l^*} \mathrm{e}^{-x/2} L_{n_r}^{2l^*+1}(x); \quad (8)$$

$$N = \sqrt{\frac{\Gamma(n_r + 2l^* + 2)}{n_r!}}, \qquad x = \frac{2Zr}{n^*},$$

where $\Gamma(\cdot)$ is the Γ function. The effective principal quantum number n^* is connected to the energy level $E(nl_j)$ and quantum defect μ_{lj} via the Rydberg formula:

$$E(nl_j) = V_{\mathrm{ion}} - \frac{Z^2 \mathcal{R}_{\mathrm{Ag}}}{n^{*2}} = V_{\mathrm{ion}} - \frac{Z^2 \mathcal{R}_{\mathrm{Ag}}}{(n - \mu_{lj})^2}, \quad (9)$$

TABLE VIII. FMP-calculated transition dipole moments (line strengths $S_{i\rightarrow k}$, oscillator strengths $f_{i\rightarrow k}$, transition probabilities $A_{k\rightarrow i}$) between $(4d^{10})n_i f$ and $(4d^{10})n_k g$ states of Ag atom in the 1300- to 4000-cm^{-1} range. The Ritz wave numbers ν and vacuum wavelengths λ are calculated using the energy-level values from the cited references.

Transition $i \leftarrow k$	Lower level (cm^{-1})	Upper level (cm^{-1})	ν (cm^{-1})	λ (nm)	S_{ik} (a. u.)	f_{ik}	A_{ki} (s^{-1})
$4f_{\frac{5}{2}} \leftarrow 5g_{\frac{7}{2}}$	54204.73 [16]	56711.1 [16]	2506.370	3989.83	1.06×10^3	1.34	4.32×10^7
$4f_{\frac{7}{2}} \leftarrow 5g_{\frac{7}{2}}$	54204.73 [16]	56711.1 [16]	2506.370	3989.83	3.92×10^1	3.73×10^{-2}	1.60×10^6
$4f_{\frac{7}{2}} \leftarrow 5g_{\frac{9}{2}}$	54204.73 [16]	56711.1 [16]	2506.370	3989.83	1.37×10^3	1.31	7.01×10^7
$4f_{\frac{5}{2}} \leftarrow 6g_{\frac{7}{2}}$	54204.73 [16]	58054.723 [66]	3849.993	2597.41	9.57×10^1	1.87×10^{-1}	1.42×10^7
$4f_{\frac{7}{2}} \leftarrow 6g_{\frac{7}{2}}$	54204.73 [16]	58054.723 [66]	3849.993	2597.41	3.54	5.18×10^{-3}	5.25×10^5
$4f_{\frac{7}{2}} \leftarrow 6g_{\frac{9}{2}}$	54204.73 [16]	58054.723 [66]	3849.993	2597.41	1.24×10^2	1.81×10^{-1}	2.30×10^7
$5f_{\frac{5}{2}} \leftarrow 6g_{\frac{7}{2}}$	56691.275 [66]	58054.723 [66]	1363.448	7334.35	1.69×10^3	1.17	1.11×10^7
$5f_{\frac{7}{2}} \leftarrow 6g_{\frac{7}{2}}$	56691.397 [66]	58054.723 [66]	1363.326	7335.00	6.26×10^1	3.24×10^{-2}	4.11×10^5
$5f_{\frac{7}{2}} \leftarrow 6g_{\frac{9}{2}}$	56691.397 [66]	58054.723 [66]	1363.326	7335.00	2.19×10^3	1.13	1.80×10^7
$5f_{\frac{5}{2}} \leftarrow 7g_{\frac{7}{2}}$	56691.275 [66]	58864.694 [16][a]	2173.419	4601.05	2.10×10^2	2.32×10^{-1}	5.60×10^6
$5f_{\frac{7}{2}} \leftarrow 7g_{\frac{7}{2}}$	56691.397 [66]	58864.694 [16][a]	2173.297	4601.30	7.79	6.43×10^{-3}	2.07×10^5
$5f_{\frac{7}{2}} \leftarrow 7g_{\frac{9}{2}}$	56691.397 [66]	58864.694 [16,66][a]	2173.297	4601.30	2.73×10^2	2.25×10^{-1}	9.08×10^6
$5f_{\frac{5}{2}} \leftarrow 8g_{\frac{7}{2}}$	56691.275 [66]	59390.301 [16][a]	2699.026	3705.04	6.33×10^1	8.65×10^{-2}	3.23×10^6
$5f_{\frac{7}{2}} \leftarrow 8g_{\frac{7}{2}}$	56691.397 [66]	59390.301 [16][a]	2698.904	3705.21	2.35	2.40×10^{-3}	1.20×10^5
$5f_{\frac{7}{2}} \leftarrow 8g_{\frac{9}{2}}$	56691.397 [66]	59390.301 [16,66][a]	2698.904	3705.21	8.21×10^1	8.41×10^{-2}	5.23×10^6
$6f_{\frac{5}{2}} \leftarrow 8g_{\frac{7}{2}}$	58045.481 [66]	59390.301 [16][a]	1344.820	7435.94	3.61×10^2	2.46×10^{-1}	2.28×10^6
$6f_{\frac{7}{2}} \leftarrow 8g_{\frac{7}{2}}$	58040.839 [16,66][a]	59390.301 [16][a]	1349.462	7410.36	1.33×10^1	6.83×10^{-3}	8.49×10^4
$6f_{\frac{7}{2}} \leftarrow 8g_{\frac{9}{2}}$	58040.839 [16,66][a]	59390.301 [16,66][a]	1349.462	7410.36	4.66×10^2	2.39×10^{-1}	3.72×10^6

[a]Obtained by extrapolation from the cited data.

TABLE IX. FMP-calculated transition dipole moments (line strengths $S_{i\to k}$, oscillator strengths $f_{i\to k}$, transition probabilities $A_{k\to i}$) between $(4d^{10})n_i g$ and $(4d^{10})n_k f$ states of Ag atom in the 1300- to 4000-cm^{-1} range. The Ritz wave numbers ν and vacuum wavelengths λ are calculated using the energy-level values from the cited references.

Transition $i \leftarrow k$	Lower level (cm^{-1})	Upper level (cm^{-1})	ν (cm^{-1})	λ (nm)	S_{ik} (a. u.)	f_{ik}	A_{ki} (s^{-1})
$5g_{\frac{7}{2}} \leftarrow 6f_{\frac{5}{2}}$	56711.1 [16]	58045.481 [66]	1334.381	7494.11	1.56×10^{1}	7.90×10^{-3}	7.21×10^{4}
$5g_{\frac{7}{2}} \leftarrow 6f_{\frac{7}{2}}$	56711.1 [16]	58040.839 [16,66][a]	1329.739	7520.27	6.10×10^{-1}	3.08×10^{-4}	3.72×10^{3}
$5g_{\frac{9}{2}} \leftarrow 6f_{\frac{7}{2}}$	56711.1 [16]	58040.839 [16,66][a]	1329.739	7520.27	2.13×10^{1}	8.62×10^{-3}	1.30×10^{5}
$5g_{\frac{7}{2}} \leftarrow 7f_{\frac{5}{2}}$	56711.1 [16]	58854.51 [66]	2143.410	4665.46	1.63	1.33×10^{-3}	3.13×10^{4}
$5g_{\frac{7}{2}} \leftarrow 7f_{\frac{7}{2}}$	56711.1 [16]	58854.765 [66]	2143.665	4664.91	6.03×10^{-2}	4.91×10^{-5}	1.54×10^{3}
$5g_{\frac{9}{2}} \leftarrow 7f_{\frac{7}{2}}$	56711.1 [16]	58854.765 [66]	2143.665	4664.91	2.11	1.37×10^{-3}	5.39×10^{4}
$5g_{\frac{7}{2}} \leftarrow 8f_{\frac{5}{2}}$	56711.1 [16]	59384.182 [16,66][a]	2673.082	3741.00	4.27×10^{-1}	4.33×10^{-4}	1.59×10^{4}
$5g_{\frac{7}{2}} \leftarrow 8f_{\frac{7}{2}}$	56711.1 [16]	59383.409 [16,66][a]	2672.309	3742.08	1.61×10^{-2}	1.63×10^{-5}	7.96×10^{2}
$5g_{\frac{9}{2}} \leftarrow 8f_{\frac{7}{2}}$	56711.1 [16]	59383.409 [16,66][a]	2672.309	3742.08	5.63×10^{-1}	4.57×10^{-4}	2.79×10^{4}
$6g_{\frac{7}{2}} \leftarrow 8f_{\frac{5}{2}}$	58054.723 [66]	59384.182 [16,66][a]	1329.459	7521.85	7.52	3.80×10^{-3}	3.44×10^{4}
$6g_{\frac{7}{2}} \leftarrow 8f_{\frac{7}{2}}$	58054.723 [66]	59383.409 [16,66][a]	1328.686	7526.23	2.83×10^{-1}	1.43×10^{-4}	1.72×10^{3}
$6g_{\frac{9}{2}} \leftarrow 8f_{\frac{7}{2}}$	58054.723 [66]	59383.409 [16,66][a]	1328.686	7526.23	9.91	4.00×10^{-3}	6.03×10^{4}

[a]Obtained by extrapolation from the cited data.

where $V_{\text{ion}} = 61106.45$ cm^{-1} [26] stands for the ionization potential of the Ag atom whose $(4d^{10})$ core's charge is $Z = 1$; $\mathcal{R}_{\text{Ag}} = 109736.758$ cm^{-1} [27] is the mass-corrected Rydberg constant for Ag. The noninteger parameter l^* accounts for the non-Coulombic potential of the core and is connected to the principal quantum number in the following way:

$$n^* = n_r + l^* + 1. \tag{10}$$

The integer radial quantum number n_r is equal to the number of nodes of the radial wave function $R(r)$; for the Ag atom this number was determined as

$$n_r = \begin{cases} \max\{1, n-5\} & \text{for} \quad s \text{ states } (n \geqslant 5); \\ n-5 & \text{for} \quad p,d \text{ states } (n \geqslant 5); \\ n-l-1 & \text{for} \quad l \geqslant 3 \text{ states } (n \geqslant l+1). \end{cases} \tag{11}$$

TABLE X. FMP-calculated transition dipole moments (line strengths $S_{i\to k}$, oscillator strengths $f_{i\to k}$, transition probabilities $A_{k\to i}$) between $(4d^{10})n_i d$ and $(4d^{10})n_k f$ states of Ag atom in the 1300- to 4000-cm^{-1} range. The Ritz wave numbers ν and vacuum wavelengths λ are calculated using the energy-level values from the cited references.

Transition $i \leftarrow k$	Lower level (cm^{-1})	Upper level (cm^{-1})	ν (cm^{-1})	λ (nm)	S_{ik} (a. u.)	f_{ik}	A_{ki} (s^{-1})
$6d_{\frac{3}{2}} \leftarrow 5f_{\frac{5}{2}}$	54203.119 [66]	56691.275 [66]	2488.156	4019.04	4.70×10^{2}	8.88×10^{-1}	1.41×10^{7}
$6d_{\frac{5}{2}} \leftarrow 5f_{\frac{5}{2}}$	54213.564 [66]	56691.275 [66]	2477.711	4035.98	3.39×10^{1}	4.25×10^{-2}	1.00×10^{6}
$6d_{\frac{5}{2}} \leftarrow 5f_{\frac{7}{2}}$	54213.564 [66]	56691.397 [66]	2477.833	4035.78	6.78×10^{2}	8.50×10^{-1}	2.67×10^{7}
$6d_{\frac{3}{2}} \leftarrow 6f_{\frac{5}{2}}$	54203.119 [66]	58045.481 [66]	3842.362	2602.57	6.36×10^{1}	1.85×10^{-1}	7.01×10^{6}
$6d_{\frac{5}{2}} \leftarrow 6f_{\frac{5}{2}}$	54213.564 [66]	58045.481 [66]	3831.917	2609.66	4.55	8.82×10^{-3}	4.97×10^{5}
$6d_{\frac{5}{2}} \leftarrow 6f_{\frac{7}{2}}$	54213.564 [66]	58040.839 [16,66][a]	3827.275	2612.83	9.07×10^{1}	1.76×10^{-1}	1.32×10^{7}
$7d_{\frac{3}{2}} \leftarrow 6f_{\frac{5}{2}}$	56699.911 [66]	58045.481 [66]	1345.570	7431.79	8.29×10^{2}	8.47×10^{-1}	3.93×10^{6}
$7d_{\frac{5}{2}} \leftarrow 6f_{\frac{5}{2}}$	56705.435 [66]	58045.481 [66]	1340.046	7462.43	6.00×10^{1}	4.07×10^{-2}	2.81×10^{5}
$7d_{\frac{5}{2}} \leftarrow 6f_{\frac{7}{2}}$	56705.435 [66]	58040.839 [16,66][a]	1335.404	7488.37	1.22×10^{3}	8.24×10^{-1}	7.52×10^{6}
$7d_{\frac{3}{2}} \leftarrow 7f_{\frac{5}{2}}$	56699.911 [66]	58854.51 [66]	2154.599	4641.23	1.20×10^{2}	1.96×10^{-1}	2.34×10^{6}
$7d_{\frac{5}{2}} \leftarrow 7f_{\frac{5}{2}}$	56705.435 [66]	58854.51 [66]	2149.075	4653.16	8.61	9.36×10^{-3}	1.66×10^{5}
$7d_{\frac{5}{2}} \leftarrow 7f_{\frac{7}{2}}$	56705.435 [66]	58854.765 [66]	2149.330	4652.61	1.72×10^{2}	1.87×10^{-1}	4.43×10^{6}
$7d_{\frac{3}{2}} \leftarrow 8f_{\frac{5}{2}}$	56699.911 [66]	59384.182 [16,66][a]	2684.271	3725.41	3.93×10^{1}	8.01×10^{-2}	1.48×10^{6}
$7d_{\frac{5}{2}} \leftarrow 8f_{\frac{5}{2}}$	56705.435 [66]	59384.182 [16,66][a]	2678.747	3733.09	2.81	3.81×10^{-3}	1.05×10^{5}
$7d_{\frac{5}{2}} \leftarrow 8f_{\frac{7}{2}}$	56705.435 [66]	59383.409 [16,66][a]	2677.974	3734.17	5.61×10^{1}	7.60×10^{-2}	2.79×10^{6}
$8d_{\frac{3}{2}} \leftarrow 8f_{\frac{5}{2}}$	58049.973 [25]	59384.182 [16,66][a]	1334.209	7495.08	2.02×10^{2}	2.05×10^{-1}	9.34×10^{5}
$8d_{\frac{5}{2}} \leftarrow 8f_{\frac{5}{2}}$	58053.404 [25]	59384.182 [16,66][a]	1330.778	7514.40	1.45×10^{1}	9.80×10^{-3}	6.66×10^{4}
$8d_{\frac{5}{2}} \leftarrow 8f_{\frac{7}{2}}$	58053.404 [25]	59383.409 [16,66][a]	1330.005	7518.77	2.91×10^{2}	1.96×10^{-1}	1.78×10^{6}

[a]Obtained by extrapolation from the cited data.

TABLE XI. FMP-calculated transition dipole moments (line strengths $S_{i\to k}$, oscillator strengths $f_{i\to k}$, transition probabilities $A_{k\to i}$) between $(4d^{10})n_i f$ and $(4d^{10})n_k d$ states of Ag atom in 1300- to 4000-cm^{-1} range. The Ritz wave numbers ν and vacuum wavelengths λ are calculated using the energy-level values from the cited references.

Transition $i \leftarrow k$	Lower level (cm^{-1})	Upper level (cm^{-1})	ν (cm^{-1})	λ (nm)	S_{ik} (a. u.)	f_{ik}	A_{ki} (s^{-1})
$4f_{\frac{5}{2}} \leftarrow 7d_{\frac{3}{2}}$	54204.73 [16]	56699.911 [66]	2495.181	4007.73	6.36	8.04×10^{-3}	1.28×10^{5}
$4f_{\frac{5}{2}} \leftarrow 7d_{\frac{5}{2}}$	54204.73 [16]	56705.435 [66]	2500.705	3998.87	4.37×10^{-1}	5.53×10^{-4}	1.33×10^{4}
$4f_{\frac{7}{2}} \leftarrow 7d_{\frac{5}{2}}$	54204.73 [16]	56705.435 [66]	2500.705	3998.87	8.74	8.30×10^{-3}	2.66×10^{5}
$4f_{\frac{5}{2}} \leftarrow 8d_{\frac{3}{2}}$	54204.73 [16]	58049.973 [25]	3845.243	2600.62	7.28×10^{-1}	1.42×10^{-3}	5.37×10^{4}
$4f_{\frac{5}{2}} \leftarrow 8d_{\frac{5}{2}}$	54204.73 [16]	58053.404 [25]	3848.674	2598.30	5.01×10^{-2}	9.77×10^{-5}	5.56×10^{3}
$4f_{\frac{7}{2}} \leftarrow 8d_{\frac{5}{2}}$	54204.73 [16]	58053.404 [25]	3848.674	2598.30	1.00	1.47×10^{-3}	1.11×10^{5}
$5f_{\frac{5}{2}} \leftarrow 8d_{\frac{3}{2}}$	56691.275 [66]	58049.973 [25]	1358.698	7359.99	2.95×10^{1}	2.03×10^{-2}	9.59×10^{4}
$5f_{\frac{5}{2}} \leftarrow 8d_{\frac{5}{2}}$	56691.275 [66]	58053.404 [25]	1362.129	7341.45	2.02	1.40×10^{-3}	9.95×10^{3}
$5f_{\frac{7}{2}} \leftarrow 8d_{\frac{5}{2}}$	56691.397 [66]	58053.404 [25]	1362.007	7342.11	4.05×10^{1}	2.09×10^{-2}	1.99×10^{5}
$5f_{\frac{5}{2}} \leftarrow 9d_{\frac{3}{2}}$	56691.275 [66]	58862.463 [25]	2171.188	4605.77	3.51	3.86×10^{-3}	4.66×10^{4}
$5f_{\frac{5}{2}} \leftarrow 9d_{\frac{5}{2}}$	56691.275 [66]	58864.614 [25]	2173.339	4601.21	2.42×10^{-1}	2.67×10^{-4}	4.84×10^{3}
$5f_{\frac{7}{2}} \leftarrow 9d_{\frac{5}{2}}$	56691.397 [66]	58864.614 [25]	2173.217	4601.47	4.85	4.00×10^{-3}	9.68×10^{4}
$5f_{\frac{5}{2}} \leftarrow 10d_{\frac{3}{2}}$	56691.275 [66]	59388.97 [19]	2697.695	3706.87	1.04	1.42×10^{-3}	2.65×10^{4}
$5f_{\frac{5}{2}} \leftarrow 10d_{\frac{5}{2}}$	56691.275 [66]	59390.587 [25]	2699.312	3704.65	7.16×10^{-2}	9.78×10^{-5}	2.74×10^{3}
$5f_{\frac{7}{2}} \leftarrow 10d_{\frac{5}{2}}$	56691.397 [66]	59390.587 [25]	2699.190	3704.82	1.43	1.47×10^{-3}	5.48×10^{4}
$6f_{\frac{5}{2}} \leftarrow 10d_{\frac{3}{2}}$	58045.481 [66]	59388.97 [19]	1343.489	7443.31	1.07×10^{1}	7.29×10^{-3}	3.37×10^{4}
$6f_{\frac{5}{2}} \leftarrow 10d_{\frac{5}{2}}$	58045.481 [66]	59390.587 [25]	1345.106	7434.36	7.38×10^{-1}	5.03×10^{-4}	3.49×10^{3}
$6f_{\frac{7}{2}} \leftarrow 10d_{\frac{5}{2}}$	58040.839 [16,66][a]	59390.587 [25]	1349.748	7408.79	1.41×10^{1}	7.23×10^{-3}	6.74×10^{4}

[a]Obtained by extrapolation from the cited data.

IV. RESULTS AND DISCUSSION

A. Oscillator and line strengths calculation

Before using the FMP-calculated line strengths for analyzing the relative intensities of the observed IR transitions we demonstrate that the accuracy of FMP is adequate for such a task. Since oscillator strengths are more commonly available in literature than the line strengths or radial dipole transition matrix elements, our comparison with the data reported in the literature will involve the f values.

TABLE XII. FMP-calculated transition dipole moments (line strengths $S_{i\to k}$, oscillator strengths $f_{i\to k}$, transition probabilities $A_{k\to i}$) between $(4d^{10})n_i p$ and $(4d^{10})n_k d$ states of Ag atom in the 1300- to 4000-cm^{-1} range. The Ritz wave numbers ν and vacuum wavelengths λ are calculated using the energy-level values from the cited references.

Transition $i \leftarrow k$	Lower level (cm^{-1})	Upper level (cm^{-1})	ν (cm^{-1})	λ (nm)	S_{ik} (a. u.)	f_{ik}	A_{ki} (s^{-1})
$7p_{\frac{1}{2}} \leftarrow 7d_{\frac{3}{2}}$	54041.087 [66]	56699.911 [66]	2658.824	3761.06	1.22×10^{2}	4.92×10^{-1}	2.97×10^{6}
$7p_{\frac{3}{2}} \leftarrow 7d_{\frac{3}{2}}$	54121.059 [66]	56699.911 [66]	2578.852	3877.69	2.78×10^{1}	5.43×10^{-2}	6.17×10^{5}
$7p_{\frac{3}{2}} \leftarrow 7d_{\frac{5}{2}}$	54121.059 [66]	56705.435 [66]	2584.376	3869.41	2.46×10^{2}	4.83×10^{-1}	8.27×10^{6}
$7p_{\frac{3}{2}} \leftarrow 8d_{\frac{3}{2}}$	54121.059 [66]	58049.973 [25]	3928.914	2545.23	4.71	1.40×10^{-2}	3.70×10^{5}
$7p_{\frac{3}{2}} \leftarrow 8d_{\frac{5}{2}}$	54121.059 [66]	58053.404 [25]	3932.345	2543.01	4.21×10^{1}	1.26×10^{-1}	4.98×10^{6}
$8p_{\frac{1}{2}} \leftarrow 8d_{\frac{3}{2}}$	56620.876 [66]	58049.973 [25]	1429.097	6997.43	2.29×10^{2}	4.96×10^{-1}	8.65×10^{5}
$8p_{\frac{3}{2}} \leftarrow 8d_{\frac{3}{2}}$	56660.556 [66]	58049.973 [25]	1389.417	7197.26	5.27×10^{1}	5.56×10^{-2}	1.83×10^{5}
$8p_{\frac{3}{2}} \leftarrow 8d_{\frac{5}{2}}$	56660.556 [66]	58053.404 [25]	1392.848	7179.53	4.66×10^{2}	4.93×10^{-1}	2.45×10^{6}
$8p_{\frac{1}{2}} \leftarrow 9d_{\frac{3}{2}}$	56620.876 [66]	58862.463 [25]	2241.587	4461.13	4.05×10^{1}	1.38×10^{-1}	5.92×10^{5}
$8p_{\frac{3}{2}} \leftarrow 9d_{\frac{3}{2}}$	56660.556 [66]	58862.463 [25]	2201.907	4541.52	8.80	1.47×10^{-2}	1.22×10^{5}
$8p_{\frac{3}{2}} \leftarrow 9d_{\frac{5}{2}}$	56660.556 [66]	58864.614 [25]	2204.058	4537.09	7.85×10^{1}	1.31×10^{-1}	1.63×10^{6}
$8p_{\frac{1}{2}} \leftarrow 10d_{\frac{3}{2}}$	56620.876 [66]	59388.97 [19]	2768.094	3612.59	1.47×10^{1}	6.18×10^{-2}	4.04×10^{5}
$8p_{\frac{3}{2}} \leftarrow 10d_{\frac{3}{2}}$	56660.556 [66]	59388.97 [19]	2728.414	3665.13	3.12	6.46×10^{-3}	8.21×10^{4}
$8p_{\frac{3}{2}} \leftarrow 10d_{\frac{5}{2}}$	56660.556 [66]	59390.587 [25]	2730.031	3662.96	2.79×10^{1}	5.79×10^{-2}	1.10×10^{6}
$9p_{\frac{1}{2}} \leftarrow 10d_{\frac{3}{2}}$	58005.05 [19]	59388.97 [19]	1383.920	7225.85	6.81×10^{1}	1.43×10^{-1}	2.34×10^{5}
$9p_{\frac{3}{2}} \leftarrow 10d_{\frac{3}{2}}$	58027.0 [19]	59388.97 [19]	1361.970	7342.31	1.49×10^{1}	1.54×10^{-2}	4.88×10^{4}
$9p_{\frac{3}{2}} \leftarrow 10d_{\frac{5}{2}}$	58027.0 [19]	59390.587 [25]	1363.587	7333.60	1.32×10^{2}	1.37×10^{-1}	6.53×10^{5}

TABLE XIII. FMP-calculated transition dipole moments (line strengths $S_{i\to k}$, oscillator strengths $f_{i\to k}$, transition probabilities $A_{k\to i}$) between $(4d^{10})n_i d$ and $(4d^{10})n_k p$ states of Ag atom in the 1300- to 4000-cm^{-1} range. The Ritz wave numbers ν and vacuum wavelengths λ are calculated using the energy-level values from the cited references.

Transition $i \leftarrow k$	Lower level (cm^{-1})	Upper level (cm^{-1})	ν (cm^{-1})	λ (nm)	S_{ik} (a. u.)	f_{ik}	A_{ki} (s^{-1})
$6d_{\frac{3}{2}} \leftarrow 8p_{\frac{1}{2}}$	54203.119 [66]	56620.876 [66]	2417.757	4136.06	1.86×10^{1}	3.42×10^{-2}	1.71×10^{5}
$6d_{\frac{3}{2}} \leftarrow 8p_{\frac{3}{2}}$	54203.119 [66]	56660.556 [66]	2457.437	4069.28	3.01	5.61×10^{-3}	5.78×10^{4}
$6d_{\frac{5}{2}} \leftarrow 8p_{\frac{3}{2}}$	54213.564 [66]	56660.556 [66]	2446.992	4086.65	2.79×10^{1}	3.46×10^{-2}	5.31×10^{5}
$6d_{\frac{3}{2}} \leftarrow 9p_{\frac{1}{2}}$	54203.119 [66]	58005.05 [19]	3801.931	2630.24	2.31	6.67×10^{-3}	8.23×10^{4}
$6d_{\frac{3}{2}} \leftarrow 9p_{\frac{3}{2}}$	54203.119 [66]	58027.0 [19]	3823.881	2615.14	3.91×10^{-1}	1.13×10^{-3}	2.83×10^{4}
$6d_{\frac{5}{2}} \leftarrow 9p_{\frac{3}{2}}$	54213.564 [66]	58027.0 [19]	3813.436	2622.31	3.61	6.96×10^{-3}	2.59×10^{5}
$7d_{\frac{3}{2}} \leftarrow 9p_{\frac{1}{2}}$	56699.911 [66]	58005.05 [19]	1305.139	7662.02	5.91×10^{1}	5.85×10^{-2}	8.51×10^{4}
$7d_{\frac{3}{2}} \leftarrow 9p_{\frac{3}{2}}$	56699.911 [66]	58027.0 [19]	1327.089	7535.29	9.68	9.76×10^{-3}	2.93×10^{4}
$7d_{\frac{5}{2}} \leftarrow 9p_{\frac{3}{2}}$	56705.435 [66]	58027.0 [19]	1321.565	7566.79	8.99×10^{1}	6.02×10^{-2}	2.69×10^{5}
$7d_{\frac{3}{2}} \leftarrow 10p_{\frac{1}{2}}$	56699.911 [66]	58834.25 [19]	2134.339	4685.29	7.25	1.18×10^{-2}	4.57×10^{4}
$7d_{\frac{3}{2}} \leftarrow 10p_{\frac{3}{2}}$	56699.911 [66]	58849.83 [67]	2149.919	4651.34	1.21	1.98×10^{-3}	1.56×10^{4}
$7d_{\frac{5}{2}} \leftarrow 10p_{\frac{3}{2}}$	56705.435 [66]	58849.83 [67]	2144.395	4663.32	1.12×10^{1}	1.21×10^{-2}	1.43×10^{5}

While the theoretical publications report f values, the majority of the experimental studies deal with measurements of transition probabilities or lifetimes. However, f values can be extracted from the reported lifetimes according to the Eqs. (2) and (3) if the ratios between the pairs of oscillator strengths $f_{i\to k}$ (transition probabilities $A_{k\to i}$) are known, e.g., from theoretical calculations. In our comparison we used the FMP method to calculate the theoretical ratios between the transition probabilities.

The results of such comparison with the experiment and with other calculations are presented in Tables I, II, III, IV, V, VI, and VII. The overall agreement of our calculations with other results can be considered to be reasonable with the exception of the $ns \to n'p$ transitions with $n' > 5$. However, the results of other theoretical calculations for these transitions (see Table III) differs by some orders of magnitude and some are close to our results. The f values extracted from the experimental lifetimes of the $6s_{\frac{1}{2}}$ [44] and $7s_{\frac{1}{2}}$ [45] levels differ both from the f values measured by the Rozhdestvenskii hook method [41] and from our theoretical values used for the calculation of the ratios of transition probability to extract the f values. This fact suggests that the use of FMP for extracting f values from the experimental lifetimes does not alone guarantee that the extracted f values will be close to those calculated using FMP. However, this is the case for transitions between higher-excited states; see Tables II, IV, and VI. In particular, for $5p \to 5d$ transitions the f values extracted according to FMP theoretical ratios demonstrate an agreement with the FMP-calculated f values which are not worse than the f values extracted using other theoretical ratios (see Table 2 in Ref. [54]).

For the further analysis of the observed Ag lines given in the next section we made an FMP calculation of the line strengths S for transitions between the $(4d^{10})nl_j$ states in the 1300- to 5000-cm^{-1} range. These results are presented in Tables VIII, IX, X, XI, XII, XIII, XIV, and XV. We consider the data presented in the tables in this section to be the most comprehensive compilation of f values for neutral Ag.

B. Lines observed

Some parts of the observed IR emission spectra of the Ag atom are presented in Fig. 1 at 11 μs after the laser shot, when the time profile of the emission intensity is maximum for all

TABLE XIV. FMP-calculated transition dipole moments (line strengths $S_{i\to k}$, oscillator strengths $f_{i\to k}$, transition probabilities $A_{k\to i}$) between $(4d^{10})n_i s$ and $(4d^{10})n_k p$ states of Ag atom in the 1300- to 4000 cm^{-1} range. The Ritz wave numbers ν and vacuum wavelengths λ are calculated using the energy-level values from the cited references.

Transition $i \leftarrow k$	Lower level (cm^{-1})	Upper level (cm^{-1})	ν (cm^{-1})	λ (nm)	S_{ik} (a. u.)	f_{ik}	A_{ki} (s^{-1})
$7s_{\frac{1}{2}} \leftarrow 7p_{\frac{1}{2}}$	51886.954 [66]	54041.087 [66]	2154.133	4642.24	1.66×10^{2}	5.43×10^{-1}	1.08×10^{6}
$7s_{\frac{1}{2}} \leftarrow 7p_{\frac{3}{2}}$	51886.954 [66]	54121.059 [66]	2234.105	4476.07	3.21×10^{2}	1.09	4.64×10^{6}
$8s_{\frac{1}{2}} \leftarrow 9p_{\frac{1}{2}}$	55581.246 [66]	58005.05 [19]	2423.804	4125.75	7.78	2.87×10^{-2}	7.19×10^{4}
$8s_{\frac{1}{2}} \leftarrow 9p_{\frac{3}{2}}$	55581.246 [66]	58027.0 [19]	2445.754	4088.72	1.80×10^{1}	6.69×10^{-2}	3.42×10^{5}
$8s_{\frac{1}{2}} \leftarrow 10p_{\frac{1}{2}}$	55581.246 [66]	58834.25 [19]	3253.004	3074.08	1.47	7.27×10^{-3}	3.29×10^{4}
$8s_{\frac{1}{2}} \leftarrow 10p_{\frac{3}{2}}$	55581.246 [66]	58849.83 [67]	3268.584	3059.43	3.66	1.82×10^{-2}	1.66×10^{5}
$9s_{\frac{1}{2}} \leftarrow 10p_{\frac{1}{2}}$	57425.078 [25]	58834.25 [19]	1409.172	7096.37	1.65×10^{1}	3.54×10^{-2}	3.00×10^{4}
$9s_{\frac{1}{2}} \leftarrow 10p_{\frac{3}{2}}$	57425.078 [25]	58849.83 [67]	1424.752	7018.77	3.87×10^{1}	8.37×10^{-2}	1.45×10^{5}

TABLE XV. FMP-calculated transition dipole moments (line strengths $S_{i\to k}$, oscillator strengths $f_{i\to k}$, transition probabilities $A_{k\to i}$) between $(4d^{10})n_i\,p$ and $(4d^{10})n_k s$ states of Ag atom inthe 1300- to 4000-cm^{-1} range. The Ritz wave numbers ν and vacuum wavelengths λ are calculated using the energy-level values from the cited references.

Transition $i \leftarrow k$	Lower level (cm^{-1})	Upper level (cm^{-1})	ν (cm^{-1})	λ (nm)	S_{ik} (a. u.)	f_{ik}	A_{ki} (s^{-1})
$6p_{\frac{1}{2}} \leftarrow 7s_{\frac{1}{2}}$	48297.402 [25,66]	51886.954 [66]	3589.552	2785.86	5.90×10^{1}	3.22×10^{-1}	1.77×10^{6}
$6p_{\frac{3}{2}} \leftarrow 7s_{\frac{1}{2}}$	48500.804 [66]	51886.954 [66]	3386.150	2953.21	1.27×10^{2}	3.27×10^{-1}	3.21×10^{6}
$7p_{\frac{1}{2}} \leftarrow 8s_{\frac{1}{2}}$	54041.087 [66]	55581.246 [66]	1540.159	6492.84	1.99×10^{2}	4.67×10^{-1}	4.72×10^{5}
$7p_{\frac{3}{2}} \leftarrow 8s_{\frac{1}{2}}$	54121.059 [66]	55581.246 [66]	1460.187	6848.44	4.27×10^{2}	4.74×10^{-1}	8.62×10^{5}
$7p_{\frac{1}{2}} \leftarrow 9s_{\frac{1}{2}}$	54041.087 [66]	57425.078 [25]	3383.991	2955.09	6.13	3.15×10^{-2}	1.54×10^{5}
$7p_{\frac{3}{2}} \leftarrow 9s_{\frac{1}{2}}$	54121.059 [66]	57425.078 [25]	3304.019	3026.62	1.14×10^{1}	2.85×10^{-2}	2.66×10^{5}
$8p_{\frac{1}{2}} \leftarrow 10s_{\frac{1}{2}}$	56620.876 [66]	58478.047 [25]	1857.171	5384.53	1.40×10^{1}	3.96×10^{-2}	5.82×10^{4}
$8p_{\frac{3}{2}} \leftarrow 10s_{\frac{1}{2}}$	56660.556 [66]	58478.047 [25]	1817.491	5502.09	2.59×10^{1}	3.57×10^{-2}	1.01×10^{5}

the observed lines. The most prominent IR lines observed for Ag are listed in Table XVI. Their full widths at half-maxima (FWHM) are calculated from fitting to a Voigt profile, but under our conditions this profile does not differ much from the Lorentzian shape (see Ref. [28]).

We measured the emission spectrum at a different delay time, from 0 to 30 μs, after the laser shot. This allows us to measure the time profiles of the observed Ag lines. Some such profiles are shown in Fig. 2. The temporal decay of some lines is well described by exponential fitting, while some lines display nonexponential (including some "plateaux" at 20–25 μs after the laser shot) and even nonmonotonic behavior. Therefore their decay time, τ, values are estimated in Table XVI in a rough approximation; so, for essentially nonexponential decays, the standard deviation $\Delta\tau$ is of order of τ.

It should be noted that the decay times $\tau \simeq 1 - 10\,\mu$s given in Table XVI are not related to the radiative lifetimes of Ag atom levels which are at least two orders shorter [43–45]. The temporal dynamics shown in Fig. 2 is due to a complex combination of the collisional cascade repopulation of the emitting levels [28] and the transfer processes in ablation products [57].

For classification of the observed lines, we checked all the transitions in the 1300- to 3600-cm^{-1} range allowed by the electric dipole rules. In the cases of transitions with close wave numbers we chose those with greater line strengths defined by the Eq. (4). Although, due to self-absorption and nonequilibrium population dynamics in the plasma plume, the observed line intensities can display some deviations from the equilibrium values described by Eq. (1), the qualitative picture of the relative intensities of different lines should be adequately described by S values. These values for the transitions between the $(4d^{10})nl_j$-core states with $n \leqslant 10$ in the 1300 to 5000-cm^{-1} range are given in Tables VIII, IX, X, XI, XII, XIII, XIV, and XV.

After classification we can refine the energy values for some levels involved in the classified transitions. However, the standard algorithms of such refinement (i.e., least-squares fitting used in Ref. [25]) are not appropriate for our case since the number of the measured lines is less than the number of the levels involved into the transitions. To obtain the best estimates for the level energy values E_i, we performed a minimization of a sum of deviations not only between $E_i - E_j$ and the measured wave numbers but included also the deviations between some E_i and the "reference" values for these levels taken from Refs. [19,25]. The weights in the sum of squared deviations were proportional to inverse uncertainties of the corresponding wave numbers or "reference" energies. The revised energy values E_i of some Ag terms are presented in Table XVII. For the levels with $n \leqslant 6$ our values coincides with the reference values within the uncertainty intervals, but it is not the case for $n > 6$. However, we consider our values preferable since they are extracted from spectra recorded with 0.02-cm^{-1} resolution while the reference values were obtained from spectra with resolution of 0.035–0.045 cm^{-1} [25] and 0.06 cm^{-1} [19].

According to Table VIII there should be two strong lines near 2506 cm^{-1}corresponding to $4f_{\frac{5}{2}} \leftarrow 5g_{\frac{7}{2}}$ and $4f_{\frac{7}{2}} \leftarrow 5g_{\frac{9}{2}}$ transitions. The presence of only one peak in the recorded spectra can be explained by coincidence of two corresponding lines within their width. Indeed, the measured fine splitting of f states is of order of this width, 0.122 cm^{-1} for the $5f$ state and 0.245 cm^{-1} for $7f$ state, and the fine splitting for g states should be of the same order or even less. Note that we did not observed the 2502.37 cm^{-1} line reported a century ago by Paschen [11]. To obtain reliable values of the fine-splitting component of f levels one should consider transitions from these states to nd states with larger fine splitting; see Table X.

Some of these transitions lie in the 1330- to 1350-cm^{-1} range but we observed only one line near 1345 cm^{-1} while,

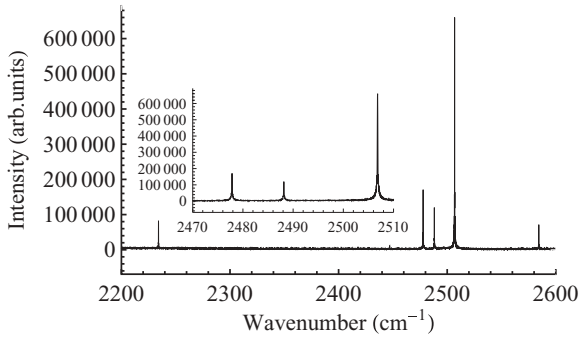

FIG. 1. A section of the the observed IR emission spectra of Ag.

TABLE XVI. Experimental Ag lines and their identification. The decay time, τ, was calculated by exponential fitting of the measured time profiles of the corresponding lines.

Wave number (cm^{-1})	Intensity (arb. units)	SNR	FWHM (cm^{-1})	Decay time (μs)	Identification
1345.570(6)	14889	14.	0.125(55)	4.17(104)[b]	$(4d^{10})7d_{\frac{3}{2}} \leftarrow (4d^{10})6f_{\frac{5}{2}}$
1363.326(14)	3910	4.3	0.146(150)	5.90(609)[b]	$(4d^{10})5f \leftarrow (4d^{10})6g$
1460.115(6)	4530	5.6	0.111(035)	3.34(170)[b]	$(4d^{10})7p_{\frac{3}{2}} \leftarrow (4d^{10})8s_{\frac{1}{2}}$
2149.320(2)	6956	2.4	0.025(19)	7.17(206)[b]	$(4d^{10})7d_{\frac{5}{2}} \leftarrow (4d^{10})7f_{\frac{7}{2}}$
2153.988(4)	32525	9.4	0.031(21)	3.07(15)	$(4d^{10})7s_{\frac{1}{2}} \leftarrow (4d^{10})7p_{\frac{1}{2}}$
2154.599(2)	5958	2.2	0.029(11)	12.8(78)[b]	$(4d^{10})7d_{\frac{3}{2}} \leftarrow (4d^{10})7f_{\frac{5}{2}}$
2234.168(1)	74835	13.	0.035(6)	3.63(34)	$(4d^{10})7s_{\frac{1}{2}} \leftarrow (4d^{10})7p_{\frac{3}{2}}$
2417.757(2)	4880	5.9	0.030(14)	5.03(214)[b]	$(4d^{10})6d_{\frac{3}{2}} \leftarrow (4d^{10})8p_{\frac{1}{2}}$
2447.045(2)	5463	6.6	0.026(24)	4.88(81)[b]	$(4d^{10})6d_{\frac{5}{2}} \leftarrow (4d^{10})8p_{\frac{3}{2}}$
2477.833(1)	113278	10.	0.044(4)	4.27(29)	$(4d^{10})6d_{\frac{5}{2}} \leftarrow (4d^{10})5f_{\frac{7}{2}}$
2488.1560(9)	78947	7.0	0.048(4)	4.20(35)[a]	$(4d^{10})6d_{\frac{3}{2}} \leftarrow (4d^{10})5f_{\frac{5}{2}}$
2506.8196(5)	460526	41.	0.056(2)	3.87(20)	$(4d^{10})4f \leftarrow (4d^{10})5g$
2579.210(3)	5252	6.2	0.036(21)	5.14(202)[b]	$(4d^{10})7p_{\frac{3}{2}} \leftarrow (4d^{10})7d_{\frac{3}{2}}$
2584.3387(6)	48450	31.	0.041(3)	4.20(37)[b]	$(4d^{10})7p_{\frac{3}{2}} \leftarrow (4d^{10})7d_{\frac{5}{2}}$
2658.7911(9)	22693	14.	0.038(5)	4.15(39)[a]	$(4d^{10})7p_{\frac{1}{2}} \leftarrow (4d^{10})7d_{\frac{3}{2}}$
3386.152(1)	98370	9.2	0.059(6)	3.35(28)	$(4d^{10})6p_{\frac{3}{2}} \leftarrow (4d^{10})7s_{\frac{1}{2}}$
3589.552(5)	13825	15.	0.065(4)	3.15(11)[a]	$(4d^{10})6p_{\frac{1}{2}} \leftarrow (4d^{10})7s_{\frac{1}{2}}$

[a]Time profile demonstrates significant deviation from the exponential decay.
[b]The decay curve has essentially nonexponential form with a plateau or a second maximum; the τ value is roughly approximate.

according to Table X, there should be two lines separated by approximately 5–10 cm^{-1}. Another unexplained feature is that, according to Table VIII, the 1363-cm^{-1} line corresponding to the $5f \leftarrow 6g$ transition should have greater intensity than the 1345-cm^{-1} line, but this is not supported by our observation. It can be due to the fact that, in our laser-ablated plasma the $6f$ and $6g$ states are less populated. It should also be noted that our spectra in the 1200- to 1800-cm^{-1} range was recorded using a MCT detector and demonstrate high level of noise. Since our data are insufficient to resolve the fine structure components of the $5f \leftarrow 6g$ transition, the value 58054.723 cm^{-1}, which is given in the Table XVII for the $6g$ state without specifying

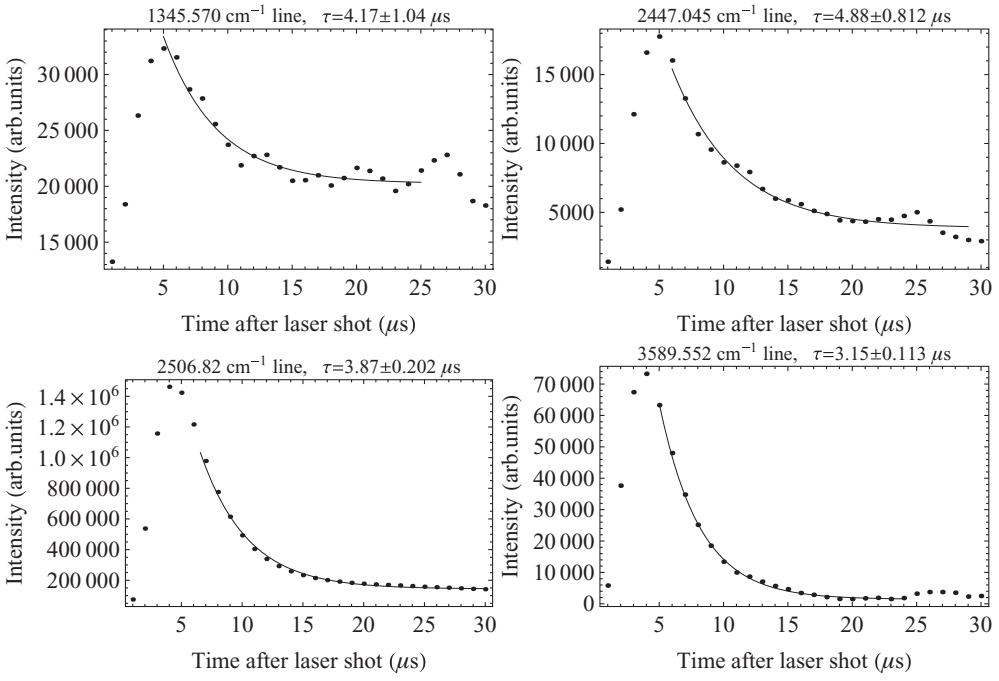

FIG. 2. The time profiles of some observed lines (dots) and their fit with exponential decay (solid curves).

TABLE XVII. Revised values of some levels of Ag I.

Term	Energy (cm^{-1})	Other sources
$(4d^{10})5f_{\frac{5}{2}}$	56691.275(2)	56691.4 [16], 56692.5 [55]
$(4d^{10})5f_{\frac{7}{2}}$	56691.397(4)	56691.4 [16], 56694.4 [55]
$(4d^{10})6p_{\frac{1}{2}}$	48297.402(2)	48297.402(3) [25]
$(4d^{10})6p_{\frac{3}{2}}$	48500.804(1)	48500.804(2) [25]
$(4d^{10})6d_{\frac{3}{2}}$	54203.119(2)	54203.119(2) [25]
$(4d^{10})6d_{\frac{5}{2}}$	54213.564(3)	54213.570(3) [25]
$(4d^{10})6f_{\frac{5}{2}}$	58045.481(7)	This work
$(4d^{10})6g$	58054.723(16)	This work
$(4d^{10})7s_{\frac{1}{2}}$	51886.954(1)	51886.971(2) [25]
$(4d^{10})7p_{\frac{1}{2}}$	54041.087(2)	54040.99(6) [19]
$(4d^{10})7p_{\frac{3}{2}}$	54121.059(2)	54121.129(5) [25]
$(4d^{10})8s_{\frac{1}{2}}$	55581.246(3)	55581.258(3) [25]
$(4d^{10})8p_{\frac{1}{2}}$	56620.876(3)	56620.72(6) [19]
$(4d^{10})8p_{\frac{3}{2}}$	56660.596(6)	56660.559(17) [25]
$(4d^{10})7d_{\frac{3}{2}}$	56699.911(2)	56699.768(3) [25]
$(4d^{10})7d_{\frac{5}{2}}$	56705.435(2)	56705.498(3) [25]
$(4d^{10})7f_{\frac{5}{2}}$	58854.510(3)	This work
$(4d^{10})7f_{\frac{7}{2}}$	58854.755(3)	This work

the j value, appears in Tables VIII and IX for both $(4d^{10})6g_{\frac{5}{2},\frac{7}{2}}$ sublevels.

V. CONCLUSION

This work continues the series of studies of emission IR spectra of metal vapors formed in ablation by pulsed laser radiation [28]. The TR FTIR spectroscopy was applied to observations of the emission arising after the irradiation of a silver target with a pulsed laser. This study extends the knowledge of the Ag spectra by reporting 12 lines not previously observed. We classify most of them as due to transitions between low Rydberg $(4d^{10})ns$, p, d, f, and g states with n between 5 and 8. The classification of the lines is performed by accounting for line strengths calculated by the Fues model potential. This method was shown to be appropriate for Ag by extensive comparison of the present calculations with the available experimental and theoretical results. These results are further extended for transitions in the observed range; the tables of oscillator strengths presented in this work are the most comprehensive report of the dipole transition matrix element between $(4d^{10})nl_j$ states of the neutral Ag atom. Revised values are given for energies of the $(4d^{10})ns_{\frac{1}{2}}$ $(n = 7,8)$, $(4d^{10})np_{\frac{1}{2},\frac{3}{2}}$ $(n = 6,7,8)$, $(4d^{10})nd_{\frac{3}{2},\frac{5}{2}}$ $(n = 6,7)$, and $(4d^{10})5f_{\frac{5}{2},\frac{7}{2}}$ states. The presented energy values for $(4d^{10})6f_{\frac{5}{2}}$, $(4d^{10})7f_{\frac{5}{2},\frac{7}{2}}$, and $(4d^{10})6g$ states have not been reported previously. We also recorded time profiles of the observed lines as a function of the delay time, from 0 to 30 μs, after the laser shot with maxima of emission intensity at 5–6 μs after the shot. The temporal decay of some lines is well described by a single-exponential function, while some lines display nonexponential (including some "plateaux" or secondary maxima at 20–25 μs after the laser shot). The approximate decay time for different lines varies in the 3- to 12-μs range.

ACKNOWLEDGMENTS

This work was financially supported by the Grant Agency of the Academy of Sciences of the Czech Republic (Grants No. IAA400400705 and KAN 100500652).

[1] J. E. Ross and L. H. Aller, Sol. Phys. **25**, 30 (1972).
[2] P. W. Merrill, Astrophys. J. **105**, 360 (1947).
[3] M. Jaschek and E. Brandi, Astron. Astrophys. **20**, 233 (1972).
[4] C. R. Cowley, T. Ryabchikova, F. Kupka, D. J. Bord, G. Mathys, and W. P. Bidelman, Mon. Not. R. Astron. Soc. **317**, 299 (2000).
[5] J. A. Johnson and M. Bolte, Astrophys. J. **579**, 616 (2002) [http://arxiv.org/abs/arXiv:astro-ph/0208375].
[6] J. J. Cowan, C. Sneden, S. Burles, I. I. Ivans, T. C. Beers, J. W. Truran, J. E. Lawler, F. Primas, G. M. Fuller, B. Pfeiffer, and K. Kratz, Astrophys. J. **572**, 861 (2002) [http://arxiv.org/abs/arXiv:astro-ph/0202429].
[7] N. Grevesse and A. Noels, Phys. Scripta **51**, 47 (1994).
[8] J. C. Pickering, Phys. Scripta **83**, 27 (1999).
[9] A. Jorissen, Phys. Scripta **112**, 73 (2004).
[10] F. Kerber, G. Nave, C. J. Sansonetti, and P. Bristow, Phys. Scripta **134**, 014007 (2009).
[11] F. Paschen, Ann. Phys. (Leipzig) **338**, 717 (1910).
[12] H. M. Randall, Astrophys. J. **34**, 1 (1911).
[13] H. A. Blair, Phys. Rev. A **36**, 1531 (1930).
[14] C. W. Hetzler, R. W. Boreman, and K. Burns, Phys. Rev. **48**, 656 (1935).
[15] E. Rasmussen, Phys. Rev. **57**, 243 (1940).
[16] A. G. Shenstone, Phys. Rev. **57**, 894 (1940).
[17] W. C. Martin and J. Sugar, J. Opt. Soc. Am. **59**, 1266 (1969).
[18] H.-U. Johannsen and R. Lincke, Z. Phys. A **272**, 147 (1975).
[19] C. M. Brown and M. L. Ginter, J. Opt. Soc. Am. **67**, 1323 (1977).
[20] A. M. Cantù, E. Jannitti, M. Mazzoni, M. Pettini, and G. Tondello, Phys. Scripta **19**, 283 (1979).
[21] J. P. Connerade, M. A. Baig, M. W. D. Mansfield, and E. Radtke, Proc. R. Soc. London A **361**, 379 (1978); J. P. Connerade and M. A. Baig, *ibid.* **365**, 253 (1979).
[22] S. Baier, M. Martins, B. R. Muller, M. Schulze, and P. Zimmermann, J. Phys. B **23**, 3095 (1990).
[23] M. Aslam Baig, A. Rashid, M. Hanif, W. Dussa, I. Ahmad, and J. Hormes, Phys. Rev. A **45**, 2108 (1992).
[24] S. Guérandel, T. Badr, M. Plimmer, P. Juncar, and M. Himbert, Eur. Phys. J. D **10**, 33 (2000); T. Badr, S. Guérandel, M. D. Plimmer, P. Juncar, and M. E. Himbert, *ibid.* **14**, 39 (2001).
[25] J. C. Pickering and V. Zilio, Eur. Phys. J. D **13**, 181 (2001).
[26] K. B. MacAdam, S. F. Dyubko, V. A. Efremov, V. G. Gerasimov, and M. P. Perepechay, J. Phys. B **42**, 085003 (2009).
[27] M. A. Baig, Phys. Rev. A **79**, 012509 (2009).

[28] S. Civiš, I. Matulková, J. Cihelka, K. Kawaguchi, V. E. Chernov, and E. Y. Buslov, Phys. Rev. A **81**, 012510 (2010).
[29] E. Hinnov and H. Kohn, J. Opt. Soc. Am. **47**, 156 (1957).
[30] N. P. Penkin and I.-Y. Y. Slavenas, Opt. Spectrosk. **15**, 9 (1963) [Opt. Spectrosc. (USSR) **15**, 3 (1963)].
[31] G. M. Lawrence, J. K. Link, and R. B. King, Astrophys. J. **141**, 293 (1965).
[32] N. L. Moise, Astrophys. J. **144**, 774 (1966).
[33] L. A. Levin and B. Budick, Bull. Am. Phys. Soc. **11**, 455 (1966).
[34] J. Z. Klose, Astrophys. J. **198**, 229 (1975).
[35] K. P. Selter and H. Kunze, Astrophys. J. **221**, 713 (1978).
[36] P. Hannaford and R. M. Lowe, Opt. Eng. **22**, 532 (1983).
[37] M. Soltanolkotabi and R. Gupta, Phys. Lett. A **96**, 399 (1983); Soltanolkotabi and R. M., Gupta, Physica B&C **123**, 386 (1984).
[38] J. Carlsson, P. Jönsson, and L. Sturesson, Z. Phys. D **16**, 87 (1990).
[39] P. S. Doidge, Spectrochim. Acta, Part B **50**, 209 (1995).
[40] D. A. Verner, P. D. Barthel, and D. Tytler, Astron. Astrophys. Suppl. Ser. **108**, 287 (1994).
[41] I.-Y. Y. Slavenas, Opt. Spectrosk. **20**, 485 (1966) [Opt. Spectrosc. (USSR) **20**, 264 (1966)].
[42] G. L. Plekhotkina, Opt. Spectrosk. **51**, 194 (1981) [Opt. Spectrosc. (USSR) **51**, 106 (1981)].
[43] J. Zhankui, P. Jönsson, J. Larsson, and S. Svanberg, Z. Phys. D **17**, 1 (1990).
[44] J. Bengtsson, J. Larsson, and S. Svanberg, Phys. Rev. A **42**, 5457 (1990).
[45] G. J. Bengtsson, P. Jönsson, J. Larsson, and S. Svanberg, ZPD **22**, 437 (1991).
[46] K.-T. Cheng and Y.-K. Kim, J. Opt. Soc. Am. **69**, 125 (1979).
[47] J. Migdałek and W. E. Baylis, J. Phys. B **11**, L497 (1978).
[48] J. Migdałek, J. Quant. Spectrosc. Ra. **20**, 81 (1978).
[49] J. Migdałek and W. E. Baylis, J. Quant. Spectrosc. Ra. **22**, 113 (1979).
[50] J. Migdałek and W. E. Baylis, Can. J. Phys. **57**, 1708 (1979).
[51] B. N. Chichkov and V. P. Shevelko, Phys. Scr. **23**, 1055 (1981).
[52] C. Lavin, M. A. Almaraz, and I. Martín, Z. Phys. D **34**, 143 (1995).
[53] I. Martín, M. A. Almaraz, and C. Lavin, Z. Phys. D **35**, 239 (1995).
[54] J. Migdałek and M. Garmulewicz, J. Phys. B **33**, 1735 (2000).
[55] U. I. Safronova, I. M. Savukov, M. S. Safronova, and W. R. Johnson, Phys. Rev. A **68**, 062505 (2003).
[56] L. Özdemir, B. Karaçoban, and G. Ürer, Indian J. Phys. **81**, 705 (2007).
[57] K. Kawaguchi, N. Sanechika, Y. Nishimura, R. Fujimori, T. N. Oka, Y. Hirahara, A. Jaman, and S. Civiš, Chem. Phys. Lett. **463**, 38 (2008).
[58] OPUS, "Opus spectroscopy software" [http://www.brukeroptics.com/opus.html].
[59] I. I. Sobelman, *Atomic Spectra and Radiative Transitions*, Springer Series in Chemical Physics, Vol. 1 (Springer–Verlag, Berlin, 1979).
[60] G. Simons, J. Chem. Phys. **60**, 645 (1974).
[61] I. Martin and G. Simons, J. Chem. Phys. **62**, 4799 (1975).
[62] P. G. Alcheev, V. E. Chernov, and B. A. Zon, J. Mol. Spectrosc. **211**, 71 (2002).
[63] N. L. Manakov, V. D. Ovsiannikov, and L. P. Rapoport, Phys. Rep. **141**, 320 (1986).
[64] V. E. Chernov, D. L. Dorofeev, I. Y. Kretinin, and B. A. Zon, Phys. Rev. A **71**, 022505 (2005); E. V. Akindinova, V. E. Chernov, I. Y. Kretinin, and B. A. Zon, *ibid.* **79**, 032506 (2009).
[65] I. S. Gradshteyn and I. M. Ryzhik, *Table of Integrals, Series, and Products*, 7th ed. (Academic Press, Orlando, FL, 2007).
[66] Table XVII, (2010), present work, Table XVII.
[67] NSU, "Electronic structure of atoms project" (2007), [http://i-portal.nsu.ru/lemma.dll?db=GROTRIAN&int=ENGLISH_VIEW&class=CMAINVIEW&templ=MAIN].